Nat. Hazards Earth Syst. Sci., 22, 2057–2079, 2022
https://doi.org/10.5194/nhess-22-2057-2022

Natural Hazards and Earth System Sciences
Open Access
EGU

Magnitude and source area estimations of severe prehistoric earthquakes in the western Austrian Alps

Patrick Oswald[1], **Michael Strasser**[1], **Jens Skapski**[2], **and Jasper Moernaut**[1]

[1]Department of Geology, University of Innsbruck, 6020 Innsbruck, Austria
[2]Risklayer GmbH, 76131 Karlsruhe, Germany

Correspondence: Patrick Oswald (oswald.patrick@gmx.net)

Received: 29 September 2021 – Discussion started: 19 October 2021
Accepted: 7 May 2022 – Published: 21 June 2022

Abstract. In slowly deforming intraplate tectonic regions such as the Alps only limited knowledge exists on the occurrence of severe earthquakes, their maximum possible magnitude, and their potential source areas. This is mainly due to long earthquake recurrence rates exceeding the time span of instrumental earthquake records and historical documentation. Lacustrine paleoseismology aims at retrieving long-term continuous records of seismic shaking. A paleoseismic record from a single lake provides information on events for which seismic shaking exceeded the intensity threshold at the lake site. In addition, when positive and negative evidence for seismic shaking from multiple sites can be gathered for a certain time period, minimum magnitudes and source locations can be estimated for paleo-earthquakes by a reverse application of an empirical intensity prediction equation in a geospatial analysis. Here, we present potential magnitudes and source locations of four paleo-earthquakes in the western Austrian Alps based on the integration of available and updated lake paleoseismic data, which comprise multiple mass-transport deposits on reflection seismic profiles and turbidites and soft-sediment deformation structures in sediment cores. The paleoseismic records at Plansee and Achensee covering the last $\sim$ 10 kyr were extended towards the age of lake initiation after deglaciation to obtain the longest possible paleoseismic catalogue at each lake site. Our results show that 25 severe earthquakes are recorded in the four lakes Plansee, Piburgersee, Achensee, and potentially Starnbergersee over the last $\sim$ 16 kyr, from which four earthquakes are interpreted to have left imprints in two or more lakes. Earthquake recurrence intervals range from ca. 1000 to 2000 years, with a weakly periodic to aperiodic recurrence behavior for the individual records. We interpret that relatively shorter recurrence intervals in the more orogen-internal archives Piburgersee and Achensee are related to enhanced tectonic loading, whereas a longer recurrence rate in the more orogen-external archive Plansee might reflect a decreased stress transfer across the current-day enhanced seismicity zone. Plausible epicenters of paleo-earthquake scenarios coincide with the current enhanced seismicity regions. Prehistoric earthquakes with a minimum moment magnitude (M_w) 5.8–6.1 have occurred around the Inn valley, the Brenner region, and the Fernpass–Loisach region and might have reached up to M_w 6.3 at Achensee. The paleo-earthquake catalogue might hint at a shift in severe earthquake activity near the Inn valley from east to west to east during postglacial times. ShakeMaps highlight that such severe earthquake scenarios do not solely impact the enhanced seismicity region of Tyrol but widely affect adjacent regions like southern Bavaria in Germany.

1 Introduction

Lake paleoseismic studies in different tectonic settings have demonstrated that seismic shaking can leave specific traces in lacustrine sedimentary archives, e.g., by basin-wide mass wasting or in situ soft-sediment deformation above a certain intensity threshold at the lake site (Avşar et al., 2016; Doughty et al., 2014; Howarth et al., 2014; Monecke et al., 2004; Petersen et al., 2014; Praet et al., 2017; Strasser et al., 2013). As glaciogenic lakes are often characterized by continuous sedimentation since deglaciation, they can have continuously recorded earthquakes since then.

Especially in slowly deforming, intraplate tectonic settings like the Alps, recurrence rates of severe earthquakes often exceed the time span of historical earthquake documentation (Beck, 2009; Brooks, 2018; Kremer et al., 2017; Moernaut, 2020; Simonneau et al., 2013). Therefore, long-term lake paleoseismic records provide valuable data to better constrain the recurrence rate and the maximum possible magnitude of severe earthquakes. However, the epicenter location, magnitude, and rupture extent of the event mostly remain unknown solely based on a lacustrine paleoseismic archive. Moreover, on-fault evidence is hardly preserved in the Alps due to penetrative anthropogenic landscape modification, gravitational slope processes, and relatively high erosion rates (Ustaszewski and Pfiffner, 2008). The so-far unraveled active faults are only discovered in special environments, such as displaced Roman archeological remains (Galadini and Galli, 1999), tectonically damaged speleothems (Plan et al., 2010), and the sedimentary infills of lakes (Fabbri et al., 2017, 2021; Gasperini et al., 2020; de La Taille et al., 2015; Oswald et al., 2021a). To date, two different ground motion modeling methods have been developed to overcome these limitations. The first method calculates potential magnitude-epicenter assemblages over a grid based on positive and negative shaking evidence of a certain intensity threshold using a backward application of an intensity prediction equation (IPE; Strasser et al., 2006; Kremer et al., 2017, after Bakun and Wentworth, 1997). The second method calculates potential source faults, the rupture length, and the magnitude in a forward modeling approach, which equally handles positive and negative shaking evidence and considers the uncertainty in the IPE (Vanneste et al., 2018). However, this method requires an accurate map of potentially active faults, which is complicated in the Alps due to the vast number of faults within a confined space for which only limited knowledge exists on their subsurface continuation and interrelation to other faults.

Recent lacustrine paleoseismological studies in the western Austrian Alps retrieved three continuous paleoseismic archives covering the Holocene (Oswald et al., 2021a, b). This study aims to extend these existing paleoseismic records in the western Austrian Alps towards the timing of lake initiation where applicable. We compare the timing and relative imprint size of earthquake-related deposits. Based on this we evaluate potential single-earthquake events with multiple lake imprints and calculate recurrence statistics on the paleo-earthquake catalogue of the region. Furthermore, we provide possible earthquake parameters of paleo-earthquakes that can explain the observational sedimentological evidence in the lakes and discuss our results in the context of seismicity in intraplate tectonic settings.

2 Setting

The study area is located within the western Austrian Alps mainly composed of Austroalpine basement units in the south of the thin-skinned nappe stack of the Northern Calcareous Alps (Fig. 1). Towards the north, the Northern Calcareous Alps superimpose the Helvetic units, the Rhenodanubian flysch, and the Alpine foreland molasse. Penninic and sub-Penninic units outcrop in the Tauern window and the Engadin window in the southeastern and the southwestern study area, respectively. The tectonic units are divided by deep-reaching crustal faults, e.g., the Inntal shear zone, Fernpass–Loisach fault system, or the Brenner Fault (Eisbacher and Brandner, 1996; Mancktelow et al., 2015; Ortner et al., 2006). These faults were mainly active together with the Periadriatic Fault south of the study area in Cenozoic times caused by north-northwestward indentation of the Adriatic microplate in the south and slab rollback in the eastern Pannonian basin leading to lateral escape tectonics (Ratschbacher et al., 1991; Rosenberg et al., 2004). GPS measurements show that the Adriatic microplate is still pushing northward with about 1–2 mm yr^{-1} (Métois et al., 2015), causing moderate seismicity with dominant N–S thrust faulting mechanisms focused in a 100 km wide E–W zone in the Inn valley (Fig. 1; Reiter et al., 2018). This zone of enhanced seismicity also hosted a few historically documented devastating earthquakes (Hammerl, 2017; Hammerl et al., 2012; Stucchi et al., 2013). Despite these earthquakes only reaching moderate moment magnitudes M_w of $\sim$ 5.3–5.7, their impact was considerable due to their relatively shallow depths (5–10 km; Reiter et al., 2018), leading to epicentral intensities of I_0 = VII–VIII. The strongest historical earthquake in Hall (1670 CE) reached M_w 5.7 ± 0.5 (Stucchi et al., 2013) and caused very strong to severe damage (I = VII–VIII) in the surrounding municipalities within approximately 120 km^2. Moreover, this event was moderately felt (I = V) up to the 250 km distant Nuremberg and lightly felt with I = IV in Salzburg (130 km). However, the exact intensity distribution caused by the Hall earthquake is unknown due to the scarceness of macroseismic reports (Hammerl et al., 2012; Stucchi et al., 2013). For the historical M_w 5.3 Namlos earthquake (1930 CE), enough earthquake information exists in the form of public macroseismic reports to characterize its regional impact (Fig. 2; Oswald et al., 2021b). The Namlos earthquake reached intensities of VII–VIII in an area of ca. 75 km^2 around the epicenter and was moderately felt (I = V) in an area of ca. 2500 km^2. None of the historical earthquakes has reached the maximum credible magnitude of M_w 6 (+0.5 if a strike slip mechanism is involved) estimated from worldwide fault geometry–magnitude relationships and macroseismic data (Lenhardt et al., 2007).

Recent studies established three paleoseismic records in the study area spanning the last 10 kyr by hydroacoustic imaging of the lake subsurface and multi-proxy sediment core analyses in the lakes Plansee, Piburgersee, and Achensee (Fig. 1; Oswald et al., 2021a, b). The hydroacoustic data sets contain multibeam bathymetry data of all lakes and reflection seismic profiles in the amount of 232 km at Achensee (99 km sparker source, 133 km pinger source) and

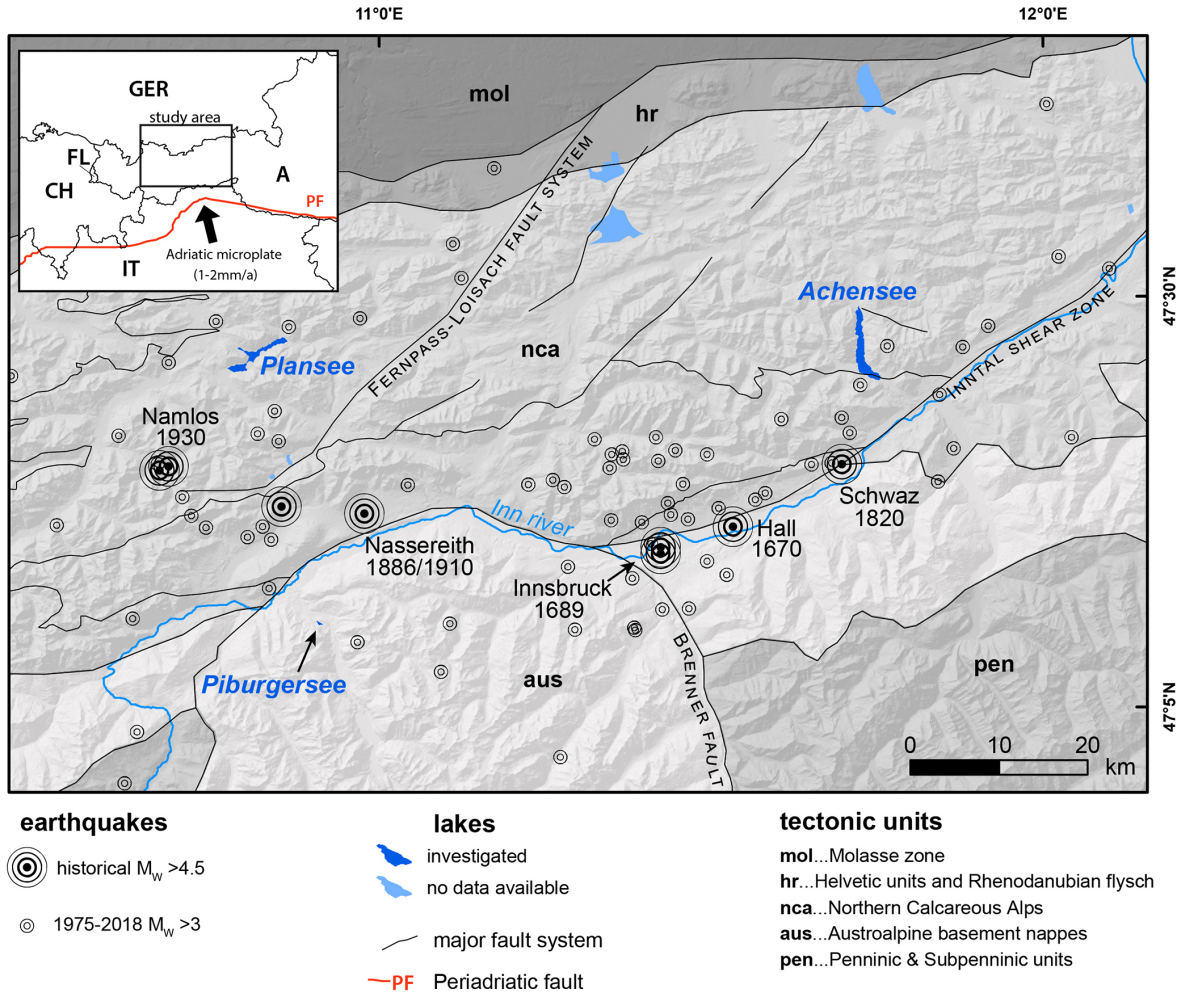

Figure 1. Overview map of the study area. The investigated lakes are located within the Northern Calcareous Alps and Austroalpine basement units subdivided and dissected by large-scale fault systems. Recent seismicity is concentrated in a 100 km wide E–W-oriented zone around the Inn valley and along the Fernpass–Loisach fault system. Severe historical earthquakes are also documented in these regions. Earthquake data derived from Stucchi et al. (2013) and Reiter et al. (2018). Inset map shows northward indentation of the Adriatic microplate into the Eastern Alps delimited by the Periadriatic Fault (PF). The study area (black rectangle) is located in western Austria (A) and surrounded by Germany (GER), Italy (IT), Switzerland (CH), and Liechtenstein (FL).

45 km (pinger source) at Plansee. Two long cores were analyzed at Achensee (10.9 and 8.1 m length), one long core from Plansee (14.3 m length), and one long core from Piburgersee (8.0 m length). Age control was obtained by radiocarbon dating and short-lived radionuclide data (^{210}Pb/^{137}Cs; Table S1 in the Supplement).

All three lakes have a glaciogenic origin, i.e., an overdeepened and underfilled valley for Achensee and Plansee, and a glacially formed hanging valley for Piburgersee. Late Glacial sedimentation is characterized by pure clastic sedimentation with enhanced sedimentation rates in a glaciolacustrine environment (for the cored sequence in Plansee of 0.15 cm yr^{-1}, Achensee of 0.24 cm yr^{-1}, and Piburgersee of 0.04 cm yr^{-1}). In Holocene times, sedimentation style is mixed hemipelagic-clastic in Plansee and Achensee due to the numerous alluvial fans bordering the lakes, and mean sedimentation rates of 0.045 and 0.034 cm yr^{-1} were obtained, respectively. In Piburgersee, Holocene sedimentation is characterized by organic-rich mud with abundant macro-organic remains and relatively low sedimentation rates (0.025 cm yr^{-1}). In the relatively deep and large lakes Plansee (68 m depth, 4.24 km^2 area) and Achensee (134 m depth, 6.8 km^2 area), seismic-stratigraphic horizons with multiple coeval mass-transport deposits (MTDs) directly overlain by a (mega-)turbidite were produced by basin-wide subaqueous mass wasting, which is interpreted to be triggered by strong earthquake shaking (cf. Praet et al., 2017; Schnellmann et al., 2002; Strasser et al., 2013). In the shallow and comparably small lake Piburgersee (24 m depth, 0.14 km^2 area), in situ soft-sediment deformation structures

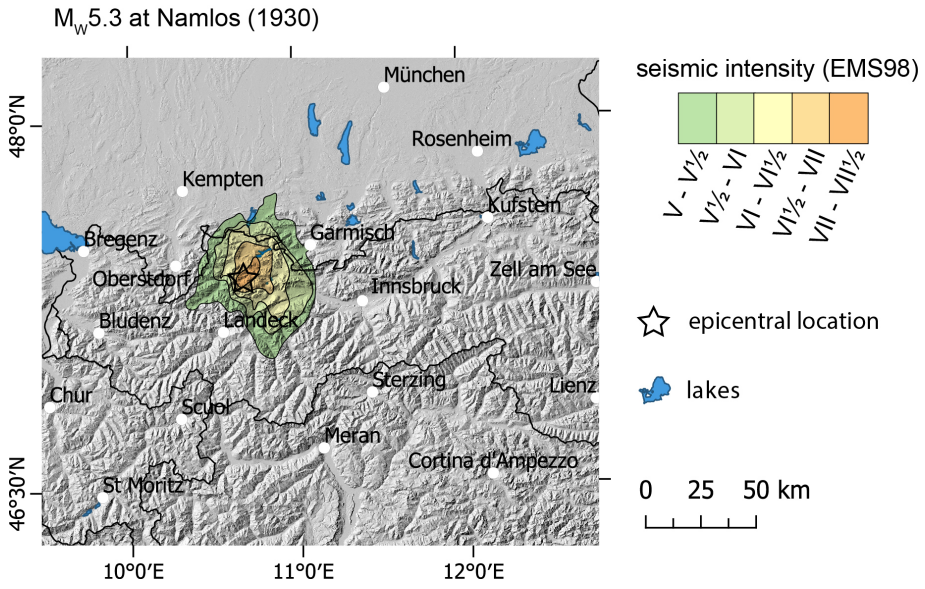

Figure 2. Isoseismal map of the historical M_W 5.3 Namlos earthquake in 1930 based on historical intensity data points (Oswald et al., 2021b).

(SSDSs) ranging from folded layers to intraclast breccia layers were observed in the flat central basin and were interpreted as signatures of strong seismic shaking (Oswald et al., 2021b).

3 Methods

3.1 Extension of the paleoseismic records and event scaling

The paleoseismic records of Plansee and Achensee are extended further back in time by (i) the investigation of outstanding turbidite deposits within the glaciolacustrine sediments by visual analyses of X-ray computer tomographic (CT) and core image data in deeper core sections (only Plansee) and by (ii) extending the age–depth models beyond the reach of the core towards initiation of glaciolacustrine sedimentation interpreted on seismic data, which allows the timing of multiple coeval MTD horizons to be estimated. The sediment depth between the base of the core and the interpreted horizon of the onset of glaciolacustrine sedimentation is calculated using the two-way travel time (TWT) in seismic data and a mean acoustic velocity of the glaciolacustrine seismic unit ($\sim 1610\,\mathrm{m\,s^{-1}}$) derived from P-wave velocity measurements on the 12–15 m subsurface depth interval of the cores that recovered the upper part of the glaciolacustrine unit. For the age–depth modeling, we used the broad age range 15–17 ka as input age for the onset of glaciolacustrine sedimentation, based on the age bracketing of glacier readvancement ($\sim$ 17 ka) and their final moraine termination ($\sim$ 15 ka; Ivy-Ochs et al., 2008). This results in the extension of the pre-existing age–depth models (Oswald et al., 2021a, b) covering the entire sequence of glaciolacustrine and lacustrine sedimentation from the deglaciation of the basin to the present day.

Age–depth models from the long cores Plan18-L1 at Plansee and ACH19-L3 at Achensee (Oswald et al., 2021a, b) are based on a combination of short-lived radionuclides (^{210}Pb and ^{137}Cs) and radiocarbon dates (Table S1) and calculated using the R package Bacon version 2.5.0 (Blaauw and Christen, 2011). For the age–depth modeling, event deposits with thicknesses of > 5 cm are deleted to obtain an event-free sediment depth. In order to also obtain an event-free sediment depth for the calculated sediment depth below the reach of the core, we assume a constant sedimentation rate and comparable number and thickness of event deposits as in the cored section of glaciolacustrine sediments.

In principle, an earthquake causes a specific sedimentary imprint when a certain, lake-specific seismic intensity threshold is exceeded (e.g., Monecke et al., 2004; Van Daele et al., 2015). Above this threshold, measurements of the sedimentary imprints such as outstanding turbidite thickness (Moernaut et al., 2014) or the occurrence of postseismic landscape response (Howarth et al., 2016) might actually indicate much higher intensities. Therefore, the inferred earthquake events are relatively scaled above the lake's individual intensity threshold based on their imprint size. The largest measured sedimentary imprint in each record corresponds to a value of 1. For Piburgersee, SSDSs are scaled based on three development stages ranging from folded layer, incipient breccia to intraclast breccia with increasing intensity (Molenaar et al., 2021; Oswald et al., 2021b; Wetzler et al., 2010) including the deposit thickness and a normalization to the range 0 to 1. The event scaling of SSDSs from a single sediment core might contain indeterminable uncertainties as the

development stage and thickness of SSDSs might vary laterally (e.g., Alsop and Marco, 2011), and the formational processes are not fully understood. At Plansee and Achensee, events are relatively scaled based on the MTD volume (V) and turbidite thickness (T) as follows: in a first step, V is divided by the slope area (A_{slope}), and T is divided by the ratio of A_{slope} to basin area (A_{basin}) to make the imprints of several lakes with different morphometric characteristics comparable (Eqs. 1 and 2).

$$V_{\text{corr}} = \frac{V}{A_{\text{slope}}} \tag{1}$$

$$T_{\text{corr}} = \frac{T}{A_{\text{slope}}/A_{\text{basin}}} \tag{2}$$

V is obtained from mapping MTDs in reflection seismic data, A_{slope} and A_{basin} are derived from spatial analysis of bathymetric data, and T is measured from the sediment core. The total MTD volume is strongly dependent on the slope area but does not change with basin area. The turbidite thickness is dependent on both the slope and the basin area because, for example, a small depocenter surrounded by large slopes would result in a relatively thicker turbidite. To calculate a scaled sedimentary imprint $\text{SED}_{\text{scaled}}$, the morphometrics-corrected MTD volume (V_{corr}) and turbidite thickness (T_{corr}) are normalized to the range 0 to 1, where the largest V_{corr} and T_{corr} corresponds to a value of 1, and summed up. Along the Alpine Fault in New Zealand, postseismic landscape response was documented to indicate one to two intensity levels higher than events that lack such response (Howarth et al., 2016), but in our case study there is no quantitative data to confidently determine this value for incorporation in the event scaling. In order to also add the occurrence of postseismic landscape response (L) as a third parameter, we define $L = 1$ for events with postseismic landscape response and $L = 0$ for events without landscape response. In a last step, $\text{SED}_{\text{scaled}}$ of the individual records is normalized to the range of 0 to 1 for a better comparison between different paleoseismic records (Eq. 3).

$$\text{SED}_{\text{scaled}} = \frac{\left(V_{\text{corr}}i - \min(V_{\text{corr}})\right)}{\left(\max(V_{\text{corr}}) - \min(V_{\text{corr}})\right)} + \frac{\left(T_{\text{corr}}i - \min(T_{\text{corr}})\right)}{\left(\max(T_{\text{corr}}) - \min(T_{\text{corr}})\right)}(+L) \tag{3}$$

3.2 Recurrence statistics

The average earthquake recurrence interval (in years) is calculated on the interevent times obtained on each lake record. To account for dating uncertainty, interevent times are derived from all individual age–depth model simulations in the software Bacon, resulting in a range of possible recurrence intervals. For records with a relatively long open end (> 1000 years) since the last event, recurrence interval calculation is carried out once only considering the closed interevent times and a second time where an imminent event in the following year is assumed (cf. Griffin et al., 2020). In this way, we also consider the elapsed time since the last event as a minimum value for the latest interevent time. Additionally, insights into the recurrence pattern of earthquakes (i.e., aperiodicity) of the lake records are obtained from the calculation of burstiness, which is directly transformed from the coefficient of variation (CoV) representing the mean-normalized standard deviation of the interevent times (Goh and Barabási, 2008). In analogy to the recurrence interval, burstiness and CoV are calculated on interevent times derived from all age–depth model simulations of each record (Kempf and Moernaut, 2021). We subdivide recurrence patterns, where a paleoseismic record with burstiness -1 to -0.33 (CoV < 0.5) is strongly periodic, -0.33 to -0.05 (CoV 0.5–0.9) is weakly periodic, -0.05 to 0.05 (CoV 0.9–1.1) is aperiodic, and 0.05 to 1 (CoV > 1.1) is bursty. It has to be noted that our approach does not incorporate the uncertainty in the estimation of burstiness due to the limited event number; i.e., there is a tendency to underestimate the burstiness of the true population mean (Kempf and Moernaut, 2021; Williams et al., 2019). However, we consider this approach appropriate for first-order estimations, especially given the fair number of paleoseismic events (8–11) in each record and the record continuity. In addition, we calculated recurrence interval and burstiness of the regional event record, where the individual events of all three lakes, each comprising all ages of the individual age–depth model simulations, are sorted by their mean age. This has the advantage that the stratigraphic order is also retained for the recurrence rate within the individual records but samples somehow randomly between the different records. Hence, this sampling technique does not artificially overestimate the interevent times of subsequent events within an individual record, which is the case for a pure random sampling between event ages of several records. However, interevent times might be slightly underestimated when shifting from one record to another as the sampling might not be completely random due to the prior defined event order.

3.3 Source area and magnitude reconstruction of paleo-earthquakes

Reconstruction of potential source areas and magnitudes of paleo-earthquakes is based on a two-step geospatial grid-search analysis (Strasser et al., 2006, 2013; Kremer et al., 2017, after Bakun and Wentworth, 1997) reversely applying the empirical IPE developed for deep earthquakes in the Swiss Alps, which is also applicable for $> M_{\text{w}}$ 5.5 earthquakes (Fäh et al., 2011). The input parameters consist of the intensity threshold for generating lacustrine mass wasting or SSDSs, along with site coordinates of positive and negative evidence for seismic shaking that exceeds this threshold. In this study, we consider earthquake-related deposits, i.e., enhanced mass wasting or SSDSs, to be potentially coeval for the calculation of paleo-earthquake scenarios when more than 40 % of the 95 % probability density functions (PDFs)

of the event ages overlap. If a lake recorded earthquake-related deposits at the observed event period, the intensity threshold was exceeded, and the lake shows positive evidence for seismic shaking. In contrast, when no earthquake-related deposits are present in the lake record at the observed time, it is assumed that the intensity threshold was not reached, resulting in negative evidence for seismic shaking as input for the calculation of plausible magnitudes and source areas. For the studied lakes in Tyrol, the intensity threshold is defined as seismic intensity (SI) $\sim$ VI 1/4 on the European macroseismic scale (EMS-98; Grünthal, 1998), representing the mean value of the lake's individual threshold intensities (Oswald et al., 2021a, b). This intensity threshold is also similar to the threshold value VI 1/5 established for Swiss perialpine lakes (Kremer et al., 2017), which further justifies the application of the estimated threshold value SI $\sim$ VI 1/4 to all studied lakes for the reconstruction of paleo-earthquake scenarios. In a first step of the grid-search analyses, minimum magnitudes are calculated for each cell based on the positive earthquake evidence. In a second step, each cell is evaluated for the sites with negative evidence and rejected if the calculated site intensity from the magnitude of the cell exceeds the intensity threshold of a site with negative earthquake evidence (see also Kremer et al., 2017).

3.4 Calculation of paleo-earthquake ShakeMaps

For a deterministic presentation of the paleo-earthquake effects, we created ShakeMaps to show the expected seismic intensity (EMS-98) in the broader study area for selected paleo-earthquake scenarios. Therefore, we used the empiric intensity (I)–distance (d) relation (Eq. 4) for earthquakes in central Europe by Sponheuer (1960):

$$I(d) = I_0 - 3\log_{10}\left(\frac{\sqrt{h^2+d^2}}{h}\right) - 1.3\alpha\left(\sqrt{h^2+d^2}-h\right), \quad (4)$$

with an absorption coefficient α (0.002 for earthquakes in central Europe) and the expected maximum intensity I_0 from the empiric relation by Rudloff and Leydecker (2002) using estimated local magnitudes (M) and hypocentral depths (h) in Eq. (5).

$$I_0 = \frac{M + 0.154 - (0.555\log_{10}(h))}{0.636} \quad (5)$$

As these relations do not describe site effects that contribute to the expected intensity in the study area, we used the macroseismic data from regional earthquakes of central Europe recorded between 2013 and 2020 to determine site parameters a and b for each point x that describe the median intensity difference from the empirical relation (Eq. 6). In a second step, we used the intensities of historical earthquake with $M_w > 5$ in Tyrol (Stucchi et al., 2013) to estimate the difference I_d of the maximum intensity to the empirically calculated I_0. The resulting equation has the form

$$I(x) = I(d) + a(M,h,d)b(x) + I_d. \quad (6)$$

While parameter a depends on earthquake parameters, b relates to local topographic effects taken from a 1 km resolution digital elevation model. Therefore, uncertainties can be expected for topographic features < 1 km, especially narrow valleys.

4 Results

4.1 Prehistoric earthquake records in Tyrol

4.1.1 Extension of the paleoseismic records at Plansee and Achensee

Seismic data of Plansee hold 11 seismic-stratigraphic horizons of multiple coeval MTDs (A–K in Fig. 3a), of which the upper 5 each correspond to an amalgamated turbidite in the sediment core (Oswald et al., 2021b). As this assemblage of observational evidence for horizon A is linked to the severe, historic M_w 5.3 Namlos earthquake, also horizons B–E were interpreted as earthquake-induced mass-wasting events (Oswald et al., 2021b). Towards greater depths six additional horizons of multiple coeval MTDs occur in seismic data (F–K in Fig. 3a), each containing three to five MTDs in the main basin of Plansee (see the Supplement of Oswald et al., 2021b).

In the sediment core, two main types of turbidites thicker than 5 cm are observed in the glaciolacustrine clays and mapped throughout the core (Fig. S2 in the Supplement). The first turbidite type is characterized by brown- to light-gray-colored, normally graded deposits with a distinct light-colored clayey-silt cap on top and contains terrestrial macro-organic remains (Fig. 3b). In analogue to the lacustrine sedimentation, these graded turbidites are interpreted to result from lake-external detrital sediment transported into the lake during hydrological events (Kiefer et al., 2021). The second type consists of overall gray homogeneous turbidites with only a thin graded base and a distinct clayey-silt cap on top and without any macro-organic remains (Fig. 3c). These homogeneous turbidites are interpreted as sediment remobilization of lake-internal slopes (Kiefer et al., 2021; Oswald et al., 2021b). The turbidite of event J contains a 5 cm, angular dolomite gravel within a homogeneous silt matrix in the uppermost part. This gravel potentially indicates a dropstone transported within a snow avalanche on a frozen lake (cf. Vasskog et al., 2011). Additionally, based on core-to-seismic correlation, each of the seismic-stratigraphic horizons H–J correspond to a homogeneous turbidite in the 15 m long sediment core (Fig. 3a). Therefore, we interpret these homogeneous turbidites derived from lake-internal enhanced mass wasting as earthquake-related in analogue to the earthquake proxy in the Holocene lacustrine sediments in Plansee (Oswald et al., 2021b) and similar lake settings (e.g., Strasser et al., 2013). In contrast, seismic-stratigraphic horizons F and G correlate to a single or a sequence of graded and much

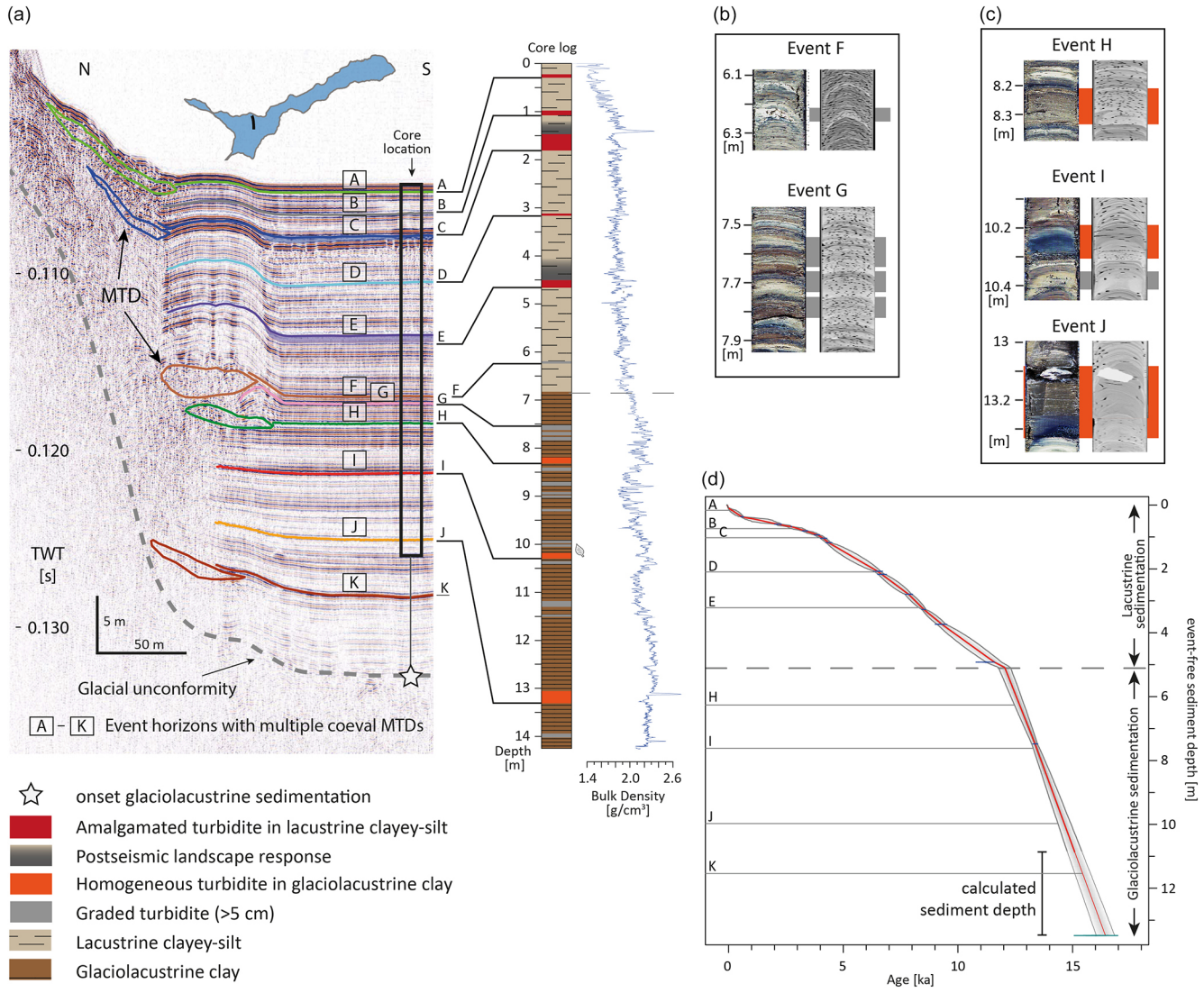

Figure 3. Extension of the paleoseismic record at Plansee. **(a)** Core-to-seismic correlation of the seismostratigraphic event horizons with multiple coeval MTDs (I–K) in seismic data to event deposits within the glaciolacustrine sediments. Correlation of event horizons A–E with amalgamated turbidites in the sediment core are derived from Oswald et al. (2021b). Core depth is extrapolated below the reach of the core to the onset of glaciolacustrine sedimentation. Inset figure shows the location of the seismic line on Plansee. **(b)** Single turbidites or a turbidite stack characterized by a normal grading and terrestrial macro-organic remains in histogram-equalized core images and CT data correlate to the seismic-stratigraphic event horizons F and G. These event horizons cannot be conclusively interpreted and either represent earthquakes or hydrological events. **(c)** Turbidites characterized by an overall homogeneous sediment body on top of a thin normally graded base in histogram-equalized core images and CT data are correlated to the seismic-stratigraphic event horizons H–J and are interpreted as earthquake-related deposits within the glaciolacustrine sediments. **(d)** Age–depth model of Plansee including calibrated ^{14}C ages from this study and Oswald et al. (2021b; Table S1) and an assumed lake initiation age (~ 15–17 ka) derived from the regional deglaciation age (Ivy-Ochs et al., 2008). Horizontal lines depict (projected) event horizons A–K. The dashed horizontal line represents the stratigraphic boundary between glaciolacustrine and lacustrine sedimentation. Sediment depths below the reach of the core (thin gray line) are calculated towards the glacial unconformity from TWT in seismic data assuming an acoustic velocity of 1610 m s^{-1}.

thinner turbidites separated by background sediment (Fig. 3a and b). The interpretation of seismic-stratigraphic horizons F and G is not unique, and they could represent either earthquakes with potentially lower intensities at the lake or hydrological events that caused onshore mass wasting within a short period. Therefore, event horizons F and G are not further used for the paleoseismic catalogue of the region.

The pre-existing age–depth model covering the Holocene is extended towards the base of glaciolacustrine sediments by adding an additional radiocarbon age in the Late Glacial at 7.5 m event-free sediment depth (Table S1 and Fig. S2)

and an inferred deglaciation age at ca. 15–17 ka at 13.5 m (Ivy-Ochs et al., 2008). This results in paleo-earthquakes at ca. 12.7, 13.4, 14.6, and 16.0 ka with 95 % age ranges of 12.5–12.9, 13.3–13.6, 14.3–14.9, and 15.6–16.4 ka, respectively (Table 1).

Achensee contains 12 seismic-stratigraphic horizons with multiple MTDs, delta collapse deposits, and (mega-)turbidites (A–L in Fig. 4a; Oswald et al., 2021a). Similar to Plansee, sedimentary earthquake imprints are expressed by the occurrence of multiple coeval MTDs in seismic data and a corresponding amalgamated turbidite because the second-youngest event horizon B was previously correlated to the historical severe $M_w \sim 5.7$ Hall earthquake in 1670 (Oswald et al., 2021a). Therefore seismic-stratigraphic horizons B–L were interpreted as earthquake-related, but only a rough age estimate (11–18 ka) was provided for the event horizons K and L, which are below the reach of the sediment cores. In contrast, the youngest event horizon A is not earthquake-related and represents a period of enhanced shoreline erosion due to anthropogenically induced lake level changes especially at the early phase of hydropower generation at Achensee.

In reflection seismic data of Achensee, lake strata are offset by subaqueous surface ruptures in prolongation of an onshore mapped fault. The upper terminations of these surface ruptures occur at three different stratigraphic levels, where each termination is directly overlain by multiple coeval MTDs (event horizons G, K, and L). This association between surface rupture and MTDs was previously interpreted as combined on-fault and off-fault paleoseismic evidence for three local severe earthquakes (Oswald et al., 2021a). The other event horizons with multiple coeval MTDs and a corresponding turbidite were interpreted as the record of remote earthquakes exceeding the intensity threshold at Achensee SI $\sim$ VI. So far, 8 of the 11 seismic-stratigraphic horizons with multiple MTDs (B–I) and 1 surface-rupturing horizon (G) are cored and dated by two 11 m long sediment cores. The extension of the age–depth model results in two local surface-rupturing events at $\sim$ 11.0 and $\sim$ 11.5 ka (K and L) and a remote earthquake at $\sim$ 10.8 ka with 95 % age ranges of 10.6–11.5, 11.0–11.9, and 10.4–11.2 ka, respectively (Table 1 and Fig. 4b).

4.1.2 The paleo-earthquake catalogue of Tyrol and its surrounding regions

The sedimentary archives of Plansee, Piburgersee, and Achensee represent the first continuous records of prehistoric earthquakes in the western Austrian Alps (Tyrol and its surrounding regions) and cover the last 16 000 years (Fig. 5a and Table 1). For each event, a qualitative intensity scaling is applied above the intensity threshold for recording earthquakes based on sedimentological criteria, such as MTD volume, turbidite thickness, development stage and thickness of SSDSs and occurrence of postseismic landscape response (Fig. 5a; Oswald et al., 2021a, b). In contrast to Plansee and Achensee, the paleoseismic record of Piburgersee is limited to the Holocene lacustrine sediments due to the lack of earthquake-induced soft-sediment deformation structures in the glaciolacustrine sediments and due to the missing seismic penetration (< 0.003 s TWT) to potentially link outstanding turbidites to multiple coeval MTDs.

The Plansee paleoseismic record (event number $n = 9$) shows the most regular recurrence pattern of the investigated records being at the boundary of "weakly periodic" and "strongly periodic" with a mean burstiness of -0.29 (range -0.40 to -0.22; Fig. 5b). It also has the largest mean recurrence interval of ca. 2000 years. The Achensee paleoseismic record ($n = 11$) is "weakly periodic" (mean burstiness -0.20, range -0.32 to -0.11) with a mean recurrence interval of ca. 1100 years. For the Piburgersee record ($n = 8$), aperiodicity and recurrence intervals are calculated in two ways to account for the relatively long earthquake quiescence since $\sim$ 3.0 ka, once considering only the closed interevent times and a second time with assuming an imminent event next year. Both calculations show a "weakly periodic" to "aperiodic" recurrence pattern (mean burstiness of -0.04 and -0.06, range of -0.16 to 0.03 and of -0.13 to 0.00) but vary in the recurrence interval with ca. 1000 and 1250 years for the closed intervals and the imminent event next year, respectively. The "real" recurrence interval at Piburgersee is potentially even longer as the imminent event will probably be further in the future. Note that the smaller scatter of burstiness and recurrence interval in the Piburgersee data set considering an imminent event next year is artificial due to the small age error in the assumed event in 2022 compared to the event ages derived from the individual age model simulations. Evaluating these recurrence statistics in light of the geographical position of the records within the Alpine orogen, the more externally situated Plansee shows the longest recurrence interval and most periodic recurrence pattern, whereas the more orogen-internal records (Piburgersee and Achensee) tend towards aperiodic recurrence behavior with about only half of the recurrence interval at Plansee. Additionally, we combine the event ages of all earthquake-related sedimentary imprints derived from the three paleoseismic records and consider the interpreted coeval events at ca. 3.0, 4.1, and 6.8 ka only once (Oswald et al., 2021b; Fig. S3). This results in 25 severe earthquakes that occurred in the study area every 630 years on average with a weakly periodic recurrence pattern.

We examined the paleo-earthquake catalogue of Tyrol presented herein (Table 1) for further overlapping event ages as this potentially indicates that a single event left traces in multiple lakes and thus impacted an area of several tens of kilometers in circumference. The assessment of a single severe earthquake from overlapping event ages requires caution because an age overlap could also be generated by two or more less strong earthquakes at different locations which occurred within a shorter time period than the error in the age–depth

Table 1. Paleoseismic events of the western Austrian Alps; their sedimentary imprints in the lakes Plansee, Piburgersee, and Achensee; and the calculated relative imprint size scale.

Lake	Earthquake ID	Event horizon	Core depth [cm]	Event-corrected depth [cm]	Modeled event ages [cal yr BP]				Turbidite/ SSDSs thickness [cm]	Off-fault paleoseismic evidence			Postseismic landscape response	SSDSs type	On-fault	Qualitative earthquake intensity	Reference
					Mean	From	To	%		MTD amount	MTD volume [m^3]	Megaturbidite volume [m^3]			Subaqueous surface rupture		
Plansee	EQ-A	A	21	16	20			–	8	12	21 000	–	–	–	–	0.16	Oswald et al. (2021b)
Plansee	EQ-B	B	96.5	73	2948	2691	3196	95	9	9	8000	–	–	–	–	0.09	Oswald et al. (2021b)
Plansee	EQ-C	C	142.5	102	4076	3961	4187	95	37	10	100 000	–	yes	–	–	1.00	Oswald et al. (2021b)
Plansee	EQ-D	D	310.5	209	6515	6372	6649	95	4	5/6	40 000	–	–	–	–	0.24	Oswald et al. (2021b)
Plansee	EQ-E	E	448.5	320.5	8422	8283	8543	95	16.5	6	17 000	–	yes	–	–	0.43	Oswald et al. (2021b)
Plansee	EQ-H	H	821	626.5	12 693	12 471	12 891	95	15	5	3700	–	–	–	–	0.10	this study
Plansee	EQ-I	I	1032	762	13 436	13 288	13 560	95	12	3	6600	–	–	–	–	0.10	this study
Plansee	EQ-J	J	1312.5	998.5	14 645	14 370	14 930	95	24	2	5000	–	–	–	–	0.16	this study
Plansee	EQ-K	K	not cored	1259.5	15 982	15 611	16 363	95	15	3	3900	–	–	–	–	0.10	this study
Piburgersee	EQ-1	1	344	75.5	3039	2716	3306	95	9	–	–	–	–	intraclast breccia	–	0.98	Oswald et al. (2021b)
Piburgersee	EQ-2	2	376.5	95.5	4133	3927	4327	95	5	–	–	–	–	incipient breccia	–	0.63	Oswald et al. (2021b)
Piburgersee	EQ-3	3	458	108	4681	4528	4871	95	4	–	–	–	–	folded layer	–	0.35	Oswald et al. (2021b)
Piburgersee	EQ-4	4	493.5	132.5	5550	5474	5636	95	10	–	–	–	–	intraclast breccia	–	1.00	Oswald et al. (2021b)
Piburgersee	EQ-5	5	517	148.5	6092	5987	6252	95	2	–	–	–	–	intraclast breccia	–	0.80	Oswald et al. (2021b)
Piburgersee	EQ-6	6	530.5	154	6258	6093	6445	95	4	–	–	–	–	intraclast breccia	–	0.85	Oswald et al. (2021b)
Piburgersee	EQ-7	7	554.5	172.5	6823	6716	6964	95	5	–	–	–	–	folded layer	–	0.38	Oswald et al. (2021b)
Piburgersee	EQ-8	8	654.5	265	9939	9767	10 133	95	6	–	–	–	–	intraclast breccia	–	0.90	Oswald et al. (2021b)
Achensee	B	B	86[a]	57[a]	267	213	296	95	22[a]	12	50 000	–	–	–	–	0.02	Oswald et al. (2021a)
Achensee	C	C	225[a]	151[a]	1012	849	1164	95	13[a]	8	15 400	–	–	–	–	0.01	Oswald et al. (2021a)
Achensee	D	D	279[a]	200[a]	2337	2213	2578	95	9[a]	6	10 300	–	–	–	–	0.01	Oswald et al. (2021a)
Achensee	E	E	386[a]	275[a]	5157	4930	5394	95	45[a]	12	165 400	50 200	–	–	–	0.07	Oswald et al. (2021a)
Achensee	F	F	505[a]	321[a]	6768	6611	6913	95	18[a]	8	45 600	–	–	–	–	0.02	Oswald et al. (2021a)
Achensee	G	G	654[a]	382[a]	8278	8180	8387	95	83[a]	5	3 404 600	189 500	–	–	Yes	1.00	Oswald et al. (2021a)
Achensee	H	H	757[a]	427[a]	8838	8723	8938	95	15[a]	9	648 700	–	–	–	–	0.18	Oswald et al. (2021a)
Achensee	I	I	859[a]	489[a]	9520	9449	9604	95	15[a]	6	683 900	24 900	–	–	–	0.20	Oswald et al. (2021a)
Achensee	J	J	1305[a, b]	653[a, b]	10 802	10 442	11 198	95	10[a, b]	3	111 500	–	–	–	–	0.03	this study
Achensee	K	K	1415[a, b]	708[a, b]	11 052	10 664	11 475	95	10[a, b]	4	96 800	–	–	–	Yes	0.03	this study
Achensee	L	L	1632[a, b]	816[a, b]	11 465	11 037	11 929	95	10[a, b]	5	57 200	–	–	–	Yes	0.02	this study

[a] Derived from long core ACH19-L7 in the main basin. [b] Event layer not cored: extrapolated depth values or assumed thickness values for quantitative intensity scaling.

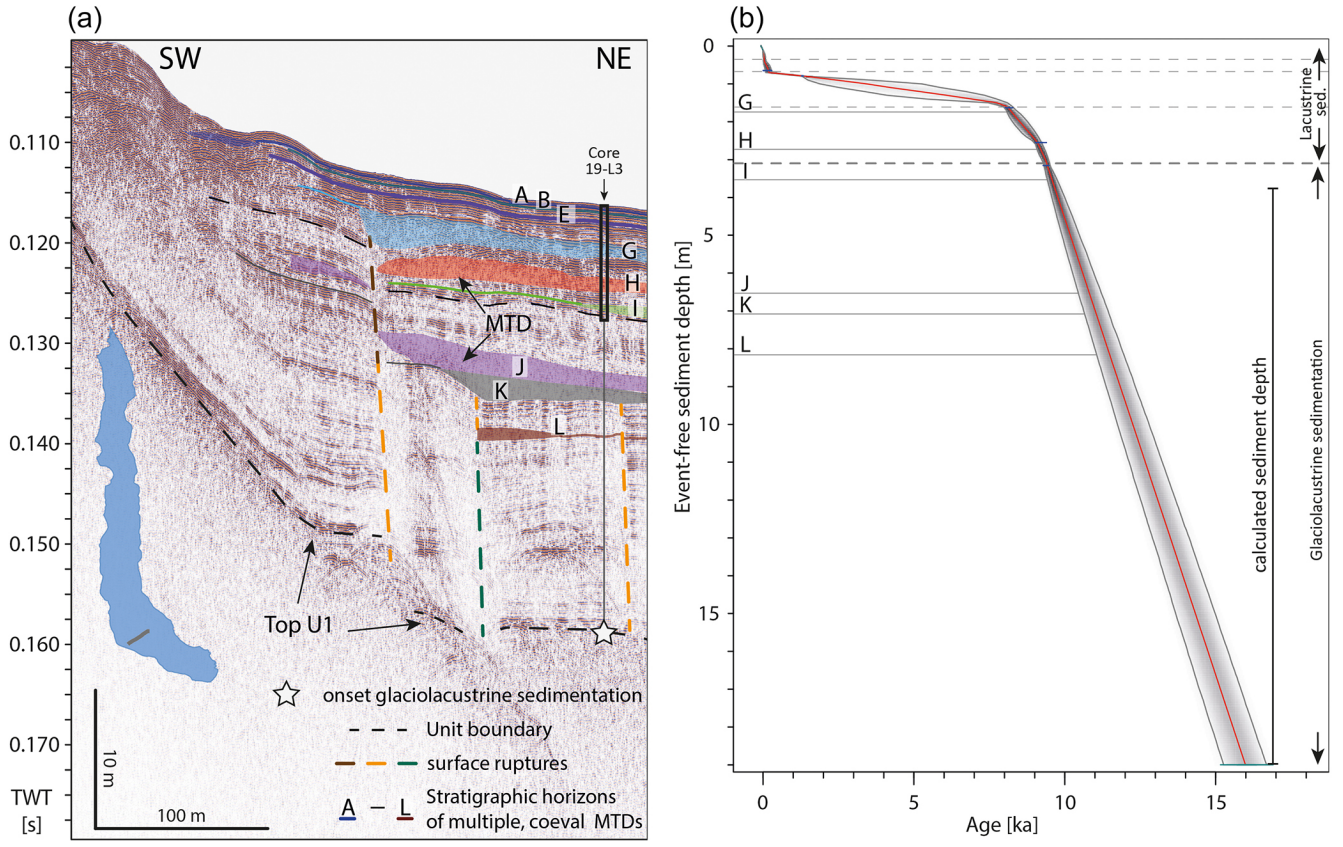

Figure 4. Extension of the paleoseismic record at Achensee. **(a)** Earthquake imprints are expressed as horizons of multiple coeval MTDs and subvertical subaqueous surface ruptures (Oswald et al., 2021a). The vertical thin gray line shows the prolongation of the previously published sediment core ACH19-L3 towards the interpreted onset of glaciolacustrine sedimentation at the top of unit 1. Inset shows the orientation of the seismic profile on Achensee. **(b)** Extension of the age–depth model of core ACH19-L3 towards the assumed begin of glaciolacustrine sedimentation (∼ 15–17 ka after Ivy-Ochs et al., 2008). Projected event-free sediment depths of event horizons J–L are marked by horizontal lines. Dashed horizontal lines represent stratigraphic boundaries. The calculated event-free sediment depth results from the depth calculation between the base of the core and the interpreted onset of glaciolacustrine sedimentation of TWT in seismic data assuming an acoustic velocity of $1610\,\mathrm{m\,s^{-1}}$.

model (Kremer et al., 2017; Oswald et al., 2021b). For the event age synchronicity evaluation, we incorporated the pre-existing surrounding lacustrine paleoseismic archives at the lakes Constance (Schwestermann, 2016), Zürich (Strasser et al., 2013; Strasser and Anselmetti, 2008), Walen (Zimmermann, 2008), Silvaplana (Bellwald, 2012), Iseo (Lauterbach et al., 2012), and Ledro (Simonneau et al., 2013; Fig. 6a) for a potential event age overlap but found only negative evidence for overlapping event ages with the three Tyrolean lakes. Moreover, the sedimentary archive of Ammersee, which was primarily investigated for its flood record, holds no paleoseismic events in the available core data of the last ∼ 5.7 kyr (Czymzik et al., 2013). At Starnbergersee, limnogeological investigations found enhanced mass wasting in seismic and core data at around 4 ka (3.7 to 4.7 ka) and in the Early Atlantic (ca. 6.5 ± 0.5 ka; Daut, 1998). As the establishment of a continuous paleoseismic record was not the focus of the study at Starnbergersee, we only consider the two mass-wasting events at ca. 4 and 6.5 ka to be potential evidence for seismic shaking (Fig. 5a) but do not extract negative evidence from this record. The paleoseismic event catalogue of the western Austrian Alps holds six periods with overlapping event ages in two records at ca. 3.0, 6.4, 6.5, 6.6, 6.8, and 8.3 ka and one period at ca. 4.1 ka with overlapping event ages in three records (Fig. 5a). A single severe event with impact on multiple lakes is very likely for the events at ∼ 3.0 (Plansee, Piburgersee) and ∼ 4.1 ka (Plansee, Piburgersee, and potentially Starnbergersee) because the 95 % PDFs of the event age ranges at Plansee and Piburgersee match well with 55 % and 45 %, respectively (Oswald et al., 2021b; Fig. S3). Additionally, potential terrestrial secondary paleoseismic evidence is documented during these periods by the occurrence of several large prehistoric rockslides (up to $1 \times 10^9\,\mathrm{m^3}$ rockslide deposit volume; Prager et al., 2008; Oswald et al., 2021b). Furthermore, a single earthquake at ca. 6.8 ka is indicated by a 68 % PDF event age overlap be-

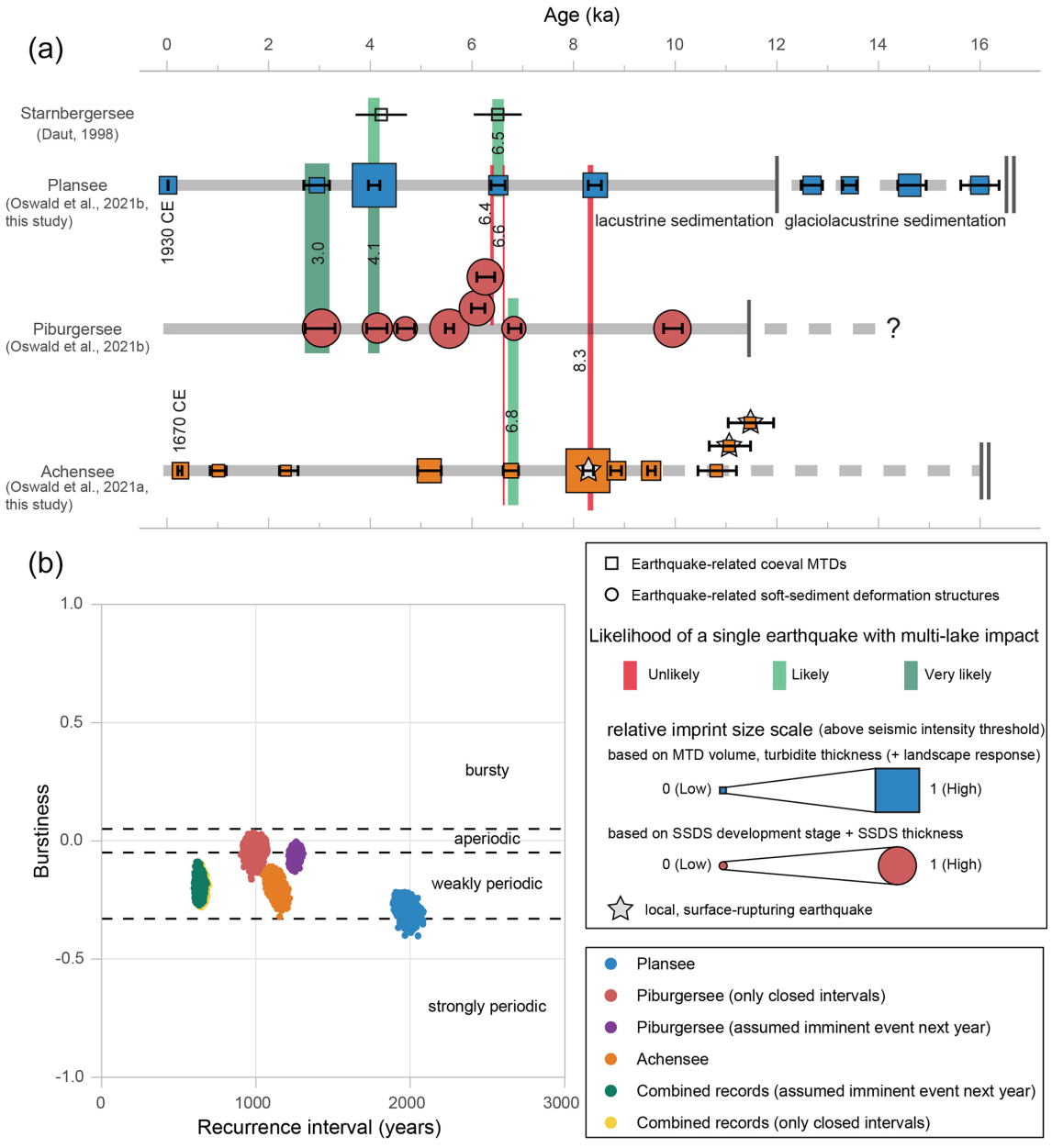

Figure 5. Lacustrine paleoseismic records of the western Austrian Alps, recurrence statistics of their paleo-earthquakes, and potential single earthquakes with impact on multiple lakes. **(a)** Timeline of the paleo-earthquakes at Plansee (this study and Oswald et al., 2021b), Piburgersee (Oswald et al., 2021b), and Achensee (this study and Oswald et al., 2021a) also including the potential earthquake-related mass-wasting events at Starnbergersee (Daut, 1998). Earthquake symbols are relatively scaled based on their imprint size above the EMS-98 intensity threshold for recording earthquakes at the lakes (cf. Oswald et al., 2021b). The likelihood assessment that these periods represent single earthquakes with an impact on multiple lakes (green–red color scale) is based on age overlaps of the individual event age PDFs (Fig. S3) and sedimentological evidence further described in the main text. Mean ages of age overlap are noted on the colored bars. Duration of lacustrine and glaciolacustrine sedimentation is indicated by continuous and dashed horizontal gray lines, respectively. **(b)** Recurrence interval–burstiness diagram of the three records calculated on all individual age–depth model simulations at the respective lake resulting in $>$ 5400 data points for each record. The recurrence interval varies from ca. 1000 to 2000 years for the individual records and is ca. 680 years for all three records combined. The burstiness shows weakly periodic to aperiodic recurrence patterns for all data sets. Note that Piburgersee is considered as two data sets given the long open end since the last event: one data set where only the closed interevent times were considered and a second data set where an imminent event is assumed in the next year.

tween lakes Piburgersee and Achensee (Fig. 5a). In the time period of ∼ 8.3 ka the PDF event age overlap at the lakes Achensee and Plansee is low (19 %), and also the observational evidence contradicts the possibility of a single event at this time. In detail, the rupture location is restricted to the Achensee area based on primary paleoseismic evidence. Within the same period, seismic shaking beyond the EMS-98 intensity threshold is indicated at Plansee by extensive mass wasting and the occurrence of postseismic landscape response, but no earthquake-related sedimentary imprint is found at Piburgersee. We also propose rejecting the possibility of a single earthquake with an imprint in multiple lakes at ca. 6.4 (Piburgersee–Plansee) and 6.6 ka (Plansee–Achensee) due to the poor PDF event age overlap of 6 % and 4 %, respectively.

4.2 Paleo-earthquake scenarios

Based on the interpreted coeval earthquake evidence in multiple lakes at ca. 3.0, 4.1, 6.5, and 6.8 ka, we investigate assemblages of potential source area and magnitude for these events under the assumption of a single earthquake event based on a reverse application of the IPE in a geospatial analysis (Fig. 6). For the following scenarios, the surrounding paleoseismic archives of the lakes Constance, Zürich, Walen, Iseo, Ledro, Silvaplana, and Ammersee (for the last ∼ 5.7 kyr) were applied as negative earthquake evidence due to missing event age overlap or no earthquake imprints at all in the case of Ammersee.

4.2.1 Scenario A at ∼ 3.0 ka

Positive earthquake evidence is present in Plansee and Piburgersee at ∼ 3.0 ka, whereas Achensee, Ammersee, and the Swiss and Italian paleoseismic archives show negative evidence (Fig. 6b). The grid-search analysis provides solutions of potential earthquake sources in the western study area with a minimum-magnitude source area in the middle between Plansee and Piburgersee around the village Nassereith with M_w 5.7 (Fig. 6b). The large prehistoric rockslides at Tschirgant and Haiming indicated as violet triangles in Fig. 6b also fall within the time range of this event and were interpreted to be earthquake-triggered (Oswald et al., 2021b). These rockslides are located slightly south of the minimum-magnitude area and much closer to Piburgersee than to Plansee. Additionally, the relative scaling of the sedimentary imprint size (0.98 at Piburgersee and 0.11 at Plansee; Table 1) indicates a much higher shaking intensity at Piburgersee than at Plansee. Therefore, we interpret the epicenter of scenario A to be more likely located south of the halfway distance between the two lakes (white line in Fig. 6b) with a minimum magnitude of M_w 5.8. Hereinafter we consider M_w 5.8 to be the minimum magnitude for scenario A and use this value for further considerations and analyses (Sect. 4.3).

4.2.2 Scenario B at ∼ 4.1 ka

At ∼ 4.1 ka, positive earthquake evidence is found in Plansee and Piburgersee and potentially in Starnbergersee, whereas Achensee, Ammersee, and the Swiss and Italian lakes show negative evidence for seismic shaking (Fig. 6c). The rockslides at Fernpass, Eibsee, and Stöttelbach (violet triangles in Fig. 6c) were previously related to this earthquake (Oswald et al., 2021b). Moreover, results from structural analyses and rock slope failure modeling in response to seismic shaking also suggest a seismic trigger for the Fernpass rockslide (Lemaire et al., 2020). The derived minimum-magnitude area and source area lie north of Garmisch-Partenkirchen with a magnitude of M_w 6.1. This event had the largest sedimentary imprint at Plansee (relative imprint scale = 1) but had only an intermediate imprint size in Piburgersee (relative imprint scale = 0.63; Table 1). This observational evidence further supports the localization of the already-small region of plausible source areas and minimum magnitudes from the grid-search analysis (Fig. 6c). It must be noted that this analysis strongly relies on the less constrained evidence at Starnbergersee. Not considering Starnbergersee as a data point would result in the same magnitude–source area distribution as in scenario A (Fig. 6b) but resulting in a minimum-magnitude estimate of M_w 6.0 around Plansee and the rockslides at ∼ 4.1 ka considering the sedimentary imprint size and the locations of the earthquake-triggered rockslides (see argumentation above).

4.2.3 Scenario C at ∼ 6.5 ka

Plansee and potentially Starnbergersee have positive evidence for seismic shaking at ∼ 6.5 ka, and negative evidence is found in the other available records (Fig. 6d). The region north of Garmisch-Partenkirchen is a potential source area with a minimum magnitude of M_w 5.9, centrally located between the two lakes, or increasingly higher if the epicenter would have been located further towards the north, west, or south. Better constraining the epicenter based on the sedimentary imprint is not feasible for this event as there are no data on the imprint size at Starnbergersee. However, the low imprint size in Plansee (0.11; Table 1) hints at an earthquake which occurred farther away. Therefore, we assume the identified minimum-magnitude area to be the most likely epicenter location for this event. Similar to scenario B, the grid-search analysis strongly relies on the less constrained evidence in Starnbergersee. In the case of falsely interpreted evidence in Starnbergersee for this event, the minimum-magnitude area would shift towards Plansee.

4.2.4 Scenario D at ∼ 6.8 ka

At ∼ 6.8 ka positive earthquake evidence is found in Achensee and Piburgersee, whereas negative evidence is derived from Plansee (Fig. 6e). The minimum-magnitude

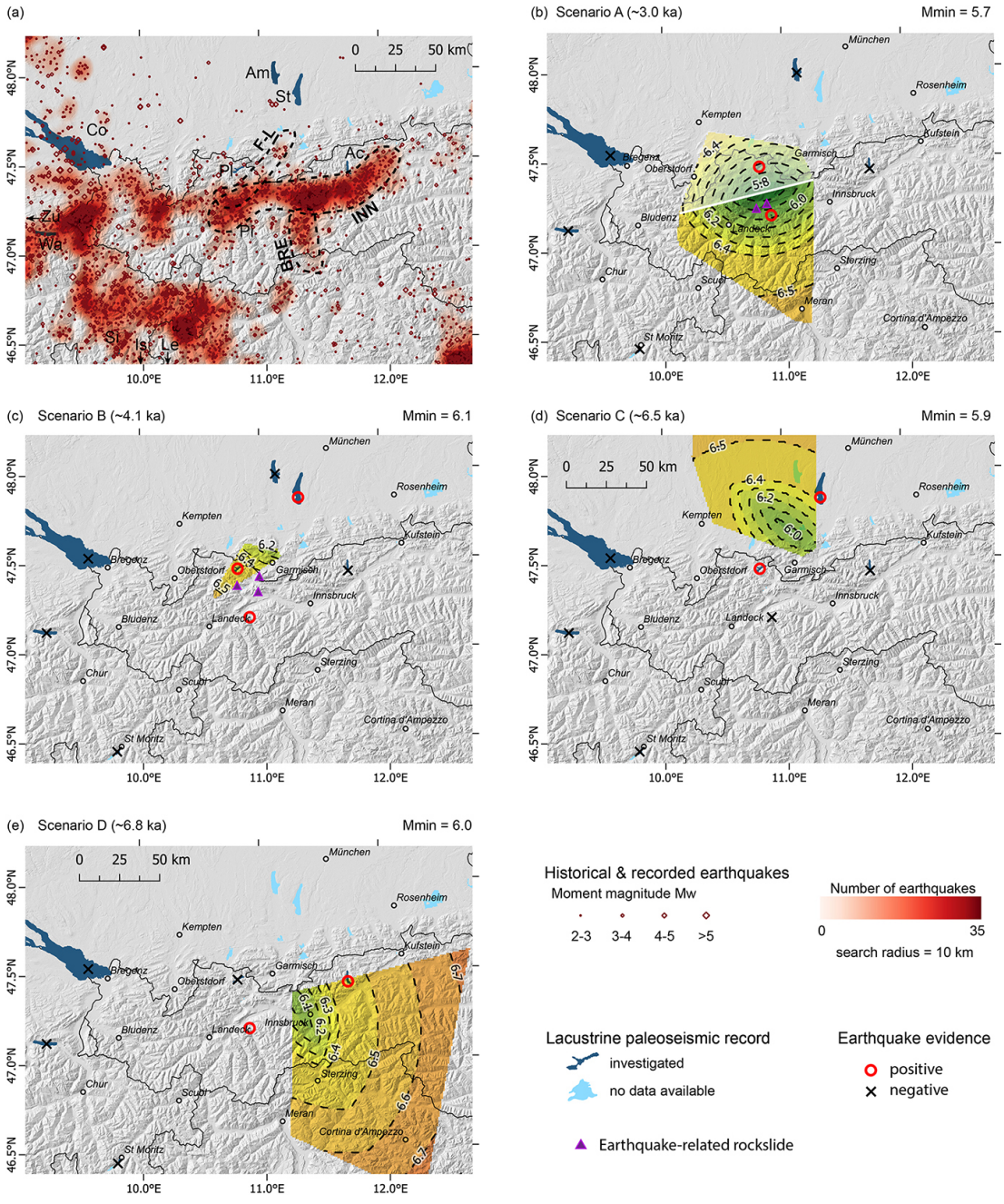

Figure 6. Magnitude and source area estimations of plausible paleo-earthquake scenarios with consideration of positive and negative earthquake evidence at multiple sites reversely using an IPE in a grid-search analysis (Strasser et al., 2006; Kremer et al., 2017, after Bakun and Wentworth, 1997). **(a)** Map with historical and instrumentally recorded earthquake data (Reiter et al., 2018; Stucchi et al., 2013); zones of present-day enhanced seismicity (dashed lines) around the Inn valley (INN), the Brenner Pass (BRE), and the Fernpass–Loisach region (F–L). The lacustrine event records investigated for the scenario modeling are Achensee (Ac; Oswald et al., 2021a), Ammersee (Am; Czymzik et al., 2013), Lake Constance (Co; Schwestermann, 2016), Lake Iseo (Is; Lauterbach et al., 2012), Lake Ledro (Le; Simonneau et al., 2013), Piburgersee (Pi; Oswald et al., 2021b), Plansee (Pl; Oswald et al., 2021b), Silvaplanasee (Si; Bellwald, 2012), Starnbergersee (St; Daut, 1998), Walensee (Wa; Zimmermann, 2008), and Lake Zürich (Zu; Strasser and Anselmetti, 2008; Strasser et al., 2013). **(b–e)** Calculated plausible source areas and minimum magnitudes for paleo-earthquakes with assumed coeval positive earthquake evidence in more than one lake at **(b)** ~ 3.0 ka, **(c)** ~ 4.1 ka, **(d)** ~ 6.5 ka, and **(e)** ~ 6.8 ka. In **(b)** and **(c)** the interpreted earthquake-related rockslides are indicated as violet triangles (Oswald et al., 2021b). Note that in **(b)** the transparent source area north of the white line is less likely due to the relatively large sedimentary imprint in Piburgersee compared to Plansee, and the earthquake-triggered rockslides further support this interpretation. Hence, the estimated source area is interpreted more in the south with a minimum magnitude of M_W 5.8, which is also used for further considerations and analysis.

source area is located around Innsbruck with a minimum magnitude estimate of M_w 6.0 and with increasing magnitudes towards the east and southeast. As both Achensee and Piburgersee have only minor sedimentary imprint sizes for this event (0.11 and 0.38, respectively; Table 1), an epicenter location farther away from both records like the area of Innsbruck or south of it is most likely.

4.3 Effects of selected paleo-earthquakes

The derived magnitudes from the modeled paleo-earthquake scenarios are well above what has been calculated from instrumental earthquake records of the last century or from historical documentation in the study area. To get a first-order idea of the consequences of such rare high-magnitude events we explore the regional shaking effects of four selected paleo-earthquake scenarios, which are reasonably constrained by our lacustrine paleoseismic data. The epicenter location of the earthquake scenarios for the ca. 3.0, 4.1, and 6.8 ka events are estimated based on the minimum-magnitude source area as revealed from the grid-search analysis. In a second step, the epicenter locations are considered more plausible closer to earthquake-triggered rockslides and lakes with higher sedimentary imprint scales (see Sect. 4.2). For the estimated epicenter area, we take the nearest town and derive the magnitude calculated from the inverse application of IPE in the grid-search analysis for the respective paleo-earthquake scenario. Besides the exploration of regional shaking effects for plausible earthquake scenarios at ca. 3.0, 4.1, and 6.8 ka, we test for the maximum possible magnitude of the surface-rupturing earthquake at Achensee at ca. 8.3 ka that did not exceed the EMS-98 intensity threshold at Piburgersee and Plansee.

A focal depth of 10 km is assumed for calculating the ShakeMaps presented in Fig. 7, which lies within the 5–15 km depth range of recent seismicity (Reiter et al., 2018). The respective calculated seismic intensities for selected towns in the broader study area are listed in Table 2.

4.3.1 Effects of a M_w 5.8 earthquake at Imst (Scenario A at ∼ 3.0 ka)

A M_w 5.8 earthquake scenario at Imst would have an epicentral intensity of VIII 1/4, and the earthquake would affect large parts of Tyrol and also areas of southern Bavaria, Baden-Württemberg, and Vorarlberg (Fig. 7a). Especially western Tyrol and the northern Alpine foreland from Kempten to Starnbergersee would be strongly affected (SI: VI to VII) in a total area of ca. 9000 km^2. The very strongly affected area with intensities > VII (∼ 550 km^2) is found around the epicenter.

4.3.2 Effects of a M_w 6.1 earthquake at Garmisch (Scenario B at ∼ 4.1 ka)

A M_w 6.1 earthquake scenario at Garmisch would have an epicentral intensity of VIII 3/4 and would affect large parts of Tyrol and southern Germany (Fig. 7b). In detail, the earthquake would be strongly felt in an area of ca. 20 000 km^2 ranging from most of Tyrol up north to Augsburg and from Lake Constance to Chiemsee. The very strongly affected area (SI: VII–VIII) would be expected in an area of ca. 5200 km^2 located in the Alpine foreland from Kempten almost to Tegernsee, up north to Ammersee, and also in the Inn valley and the Wipp valley towards the south. Severe seismic shaking is expected around the epicenter in an area of ca. 270 km^2.

4.3.3 Effects of a M_w 6.0 earthquake at Innsbruck (Scenario D at ∼ 6.8 ka)

A M_w 6.0 earthquake scenario at Innsbruck would have an epicentral intensity of VIII 1/2 and would be felt in the whole of western Austria, Bavaria, and South Tyrol (Fig. 7c). An area of ca. 14 300 km^2 is expected to be strongly affected by seismic shaking (SI: VI–VII) especially in the Inn valley, but also in the Alpine foreland from Kempten to Rosenheim. An area of 1300 km^2 in central Tyrol would experience very strong seismic shaking (SI: VII–VIII), and severe seismic intensities (SI > VIII) are expected in the Inn valley in the area of the epicenter (∼ 65 km^2).

4.3.4 Investigation of the maximum possible magnitude for the surface-rupturing earthquake at Achensee at ∼ 8.3 ka

As the ∼ 8.3 ka surface-rupturing event at Achensee is not recorded in Piburgersee or Plansee, we estimate its maximum possible magnitude by considering that the threshold intensities at Piburgersee and Plansee were not exceeded. These conditions are met for an earthquake at Achensee with a magnitude of M_w 6.3, which defines the maximum possible magnitude for the ∼ 8.3 ka surface-rupturing event. Such an event would have an epicentral intensity of VIII 3/4 and would affect large parts of western and central Austria, Bavaria, and parts of South Tyrol (Fig. 7d). In total about 30 000 km^2 is expected to be strongly affected (SI: VI–VII). In large parts of the Inn valley and southern Bavaria (ca. 8500 km^2) very strong seismic intensities (SI: VII–VIII) are expected, and severe shaking (SI > VIII) would occur in ca. 540 km^2 located in the Achensee region and the adjacent Inn and Ziller valleys. Surface ruptures are commonly present for M_w > 6.0 earthquakes (Stirling et al., 2002), which provides a minimum magnitude estimate for the surface-rupturing events at Achensee (Oswald et al., 2021a). In combination with the maximum possible magnitude from the ShakeMap (Fig. 7d) the magnitude range for the ∼ 8.3 ka surface-rupturing event at Achensee is bracketed to M_w 6.0–6.3.

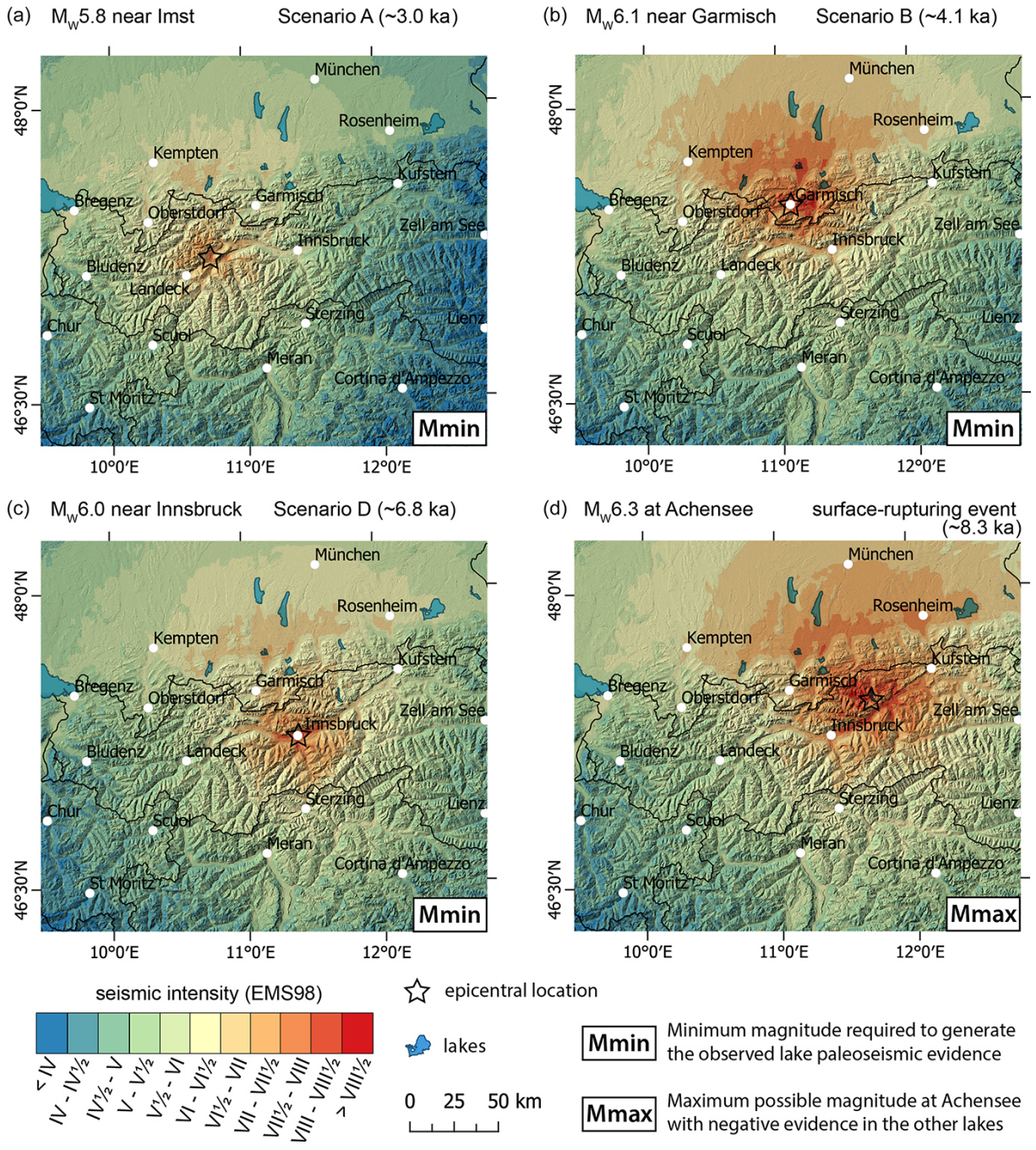

Figure 7. ShakeMaps of selected paleo-earthquake scenarios. Magnitudes and epicentral location are based on the calculated source areas and minimum magnitudes and evaluation based on the relative size of the earthquake-related sedimentary imprint and the location of earthquake-triggered rockslides (see Sect. 4.2). The ShakeMaps show seismic intensities (EMS-98) calculated for the minimum magnitude estimates of the paleo-earthquakes with presumed epicenters **(a)** near Imst at ~ 3.0 ka, **(b)** close to Garmisch-Partenkirchen at ~ 4.1 ka, and **(c)** near Innsbruck at ~ 6.8 ka. In contrast, **(d)** presents the maximum possible magnitude of M_w 6.3 for a surface-rupturing earthquake at Achensee without exceeding the seismic intensity threshold at Plansee and Piburgersee. The ShakeMaps are based on empirical relations of intensity to distance (Sponheuer, 1960) and magnitude to epicentral intensity (Rudloff and Leydecker, 2002), modified by macroseismic data of recorded earthquakes and epicentral intensities of historical events and corrected for site effects. The calculated seismic intensities at major towns for the different paleo-earthquake scenarios are provided in Table 2.

Table 2. Seismic intensities at surrounding major towns in Austria, Germany, Italy, and Switzerland for the paleo-earthquake scenarios shown in Figs. 6 and 7. Bold values indicate seismic intensities ≥ VII. Bold and italic values indicate seismic intensities ≥ VIII.

Country	Town	EMS98 seismic intensity			
		Scenario A: M_w 5.8 at Imst	Scenario B: M_w 6.1 at Garmisch-Partenkirchen	Scenario D: M_w 6.0 at Innsbruck	M_w 6.3 at Achensee (∼ 8.3 ka event)
Austria	Innsbruck	VI 1/4	**VII1/4**	***VIII1/4***	***VIII***
Austria	Kufstein	V	VI	VI	**VII1/4**
Austria	Salzburg	IV 1/2	V 3/4	V 1/2	VI 3/4
Austria	Zell am See	IV 1/2	V 1/4	V 1/2	VI 1/4
Austria	Bregenz	VI	VI 1/4	V 3/4	VI
Austria	Landeck	VI 3/4	VI	V 3/4	V 3/4
Austria	Lienz	IV	IV 3/4	V	V 3/4
Austria	Villach	III 3/4	IV 1/2	IV 3/4	V 1/2
Austria	Bludenz	V 1/4	V 1/2	V	V 1/4
Austria	Hallstatt	III	IV	IV	IV 3/4
Germany	Rosenheim	V 1/2	VI 3/4	VI 1/2	**VII1/2**
Germany	Garmisch	VI 1/2	***VIII1/2***	VI 3/4	**VII1/4**
Germany	München	V 1/2	VI 3/4	VI 1/4	**VII**
Germany	Kempten	VI 1/4	**VII**	VI 1/4	VI 1/2
Germany	Augsburg	V 1/4	VI 1/4	V 3/4	VI 1/2
Germany	Oberstdorf	VI 1/2	VI 1/2	VI	VI
Germany	Ingolstadt	IV 3/4	V 3/4	V 1/4	VI
Germany	Ulm	V 1/4	VI	V 1/4	V 3/4
Germany	Stuttgart	IV 1/4	IV 3/4	IV 1/4	IV 3/4
Italy	Sterzing	V 3/4	VI	VI 1/2	VI 1/2
Italy	Meran	V 3/4	V 3/4	VI 1/4	VI 1/4
Italy	Cortina d'Ampezzo	IV 3/4	V	V 1/2	V 3/4
Italy	Belluno	IV 1/2	V	V 1/4	V 3/4
Italy	Trento	IV 3/4	V	V 1/4	V 1/2
Italy	Tolmezzo	IV	IV 1/2	IV 3/4	V 1/2
Italy	Locarno	IV 1/2	IV 1/4	IV 1/4	IV 1/2
Switzerland	Scuol	V 1/2	V	V	V
Switzerland	Chur	IV 1/2	IV 1/2	IV 1/2	IV 1/2
Switzerland	St. Moritz	IV 1/2	IV 1/4	IV 1/4	IV 1/4

5 Discussion

5.1 Extension of paleoseismic records to Late Glacial times

In both Plansee and Achensee, the different lithologies and sedimentation rates of the glaciolacustrine and the lacustrine sediments may also affect the sensitivity of the lake acting as a natural seismograph. The earthquake proxy for multiple MTDs with a corresponding turbidite cannot be validated by historical events on site for the glaciolacustrine sediments from Late Glacial times. However, similar signatures have been successfully validated as proxies for seismic shaking in actual proglacial lakes in Alaska (Van Daele et al., 2019; Praet et al., 2017), which could be seen as analogues for the Late Glacial Achensee and Plansee. Increased sedimentation rates as present in the glaciolacustrine sediments might increase the sensitivity of the subaqueous slopes to failure (Chassiot et al., 2016; Wilhelm et al., 2016), which implies a lower intensity threshold to record seismic shaking (Praet et al., 2017). This in turn could lead to a misinterpretation of increased seismicity within Late Glacial times as a cause for the high event frequency in the Late Glacial Plansee record (ca. 820 years recurrence rate). It can be assumed that seismicity in the western Austrian Alps was enhanced in Late Glacial–Early Holocene times due to postglacial unloading and following isostatic rebound, as interpreted in other formerly glaciated regions (Beck et al., 1996; Bellwald et al., 2019; Brooks and Adams, 2020; Strasser et al., 2013). Also, the relative imprint size scaling might not be fully comparable between the Holocene and Late Glacial sediments due to different sediment properties and sedimentation dynamics. Sedimentary imprints of earthquakes might be misinterpreted as hydrological event layers in the glacio-

lacustrine sediments due to the failure of slopes predominantly influenced by clastic sedimentation. This makes it challenging to distinguish turbidites that originate from in-lake remobilization versus external fluvial sources (Praet et al., 2020). Despite the uncertainties in potential temporal changes in the intensity threshold and a potential incomplete earthquake record, the expansion of continuous paleoseismic records to their longest-possible extent is especially valuable in intraplate tectonic settings where recurrence rates are long, and paleoseismic event number is typically low, and thus little knowledge is available on recurrence patterns of severe earthquakes.

5.2 Intensity values used for the paleo-earthquake scenarios

For the calculation of potential source areas and magnitudes of paleo-earthquakes an IPE is reversely applied in a grid-search analysis using a single, uniform positive and negative intensity threshold solely on the lake records with a presumed intensity threshold of SI VI 1/4. This is due to the fact that the intensity thresholds at the individual lakes could only be determined with maximum one piece of positive evidence of a historical earthquake (Oswald et al., 2021a, b). Additionally, the magnitudes of such historical earthquakes can already have relatively large uncertainties, as is the case for the 1670 Hall earthquake (Stucchi et al., 2013), which in turn gets transferred to the intensity threshold estimation. For Piburgersee, the intensity threshold of SI VI 1/2 to VII was estimated from negative evidence of the 1930 Namlos earthquake (Oswald et al., 2021b), which also corresponds to intensity thresholds obtained in similar lake settings (Monecke et al., 2004). Moreover, due to the absence of a well-documented historical earthquake that left evidence at multiple lake sites, we are not able to test the performance of the grid-search analysis using the presumed intensity threshold (Kremer et al., 2017). The earthquake-related rockslides are not included as input data points for the grid-search analysis due to their unknown and potentially very variable intensity threshold. Though, when simply applying the environmental seismic intensity scale (ESI scale; Serva et al., 2016), rockslides with deposit volumes $> 10^7$ m^3 would indicate a seismic intensity of X, which would contradict the negative evidence found at Achensee at only 50 to 65 km distance to the potential source areas of the ~ 4.1 and ~ 3.0 ka events. This negative evidence constrains the maximum intensity at the rockslide sites to ca. SI VIII 1/2. Such a lower threshold for rockslide triggering can be explained by the relatively long-lasting interplay of hydromechanical and seismic weakening of the rock slope stability (Oswald et al., 2021b; Prager et al., 2008).

5.3 Discussion of the individual paleo-earthquake scenarios

The calculation of plausible source areas and minimum magnitudes of paleo-earthquakes assumes a single event with impact on multiple lakes. However, especially in the intraplate tectonic setting of the Alps earthquake successions or periods with enhanced seismicity are common, as exemplified by some of the strongest historical earthquakes that have occurred as clusters, e.g., six events with magnitudes ranging from M_w 5.1–6.4 within 5 months in the Friuli region in 1976 (Carulli and Slejko, 2005) and two events of M_w 5.5 to 5.7 (± 0.4) in central Tyrol in 1670 and 1689 (Stucchi et al., 2013). The time periods between these historical earthquake successions are far below the age uncertainty in radiocarbon-based age–depth models and would remain undifferentiated unless multiple consecutive earthquake imprints can be distinguished within the sedimentary record (Wils et al., 2021). Therefore, it cannot be excluded that one or the other of the presented paleo-earthquake scenarios actually represents two or more closely spaced and consecutive earthquakes with slightly smaller magnitudes.

The proposed source areas of the scenarios A (~ 3.0 ka) and D (~ 6.8 ka) are both within the zone of present-day enhanced seismicity in the area of the Inn valley and the Brenner region (Sect. 4.2 and 4.3), where large-scale fault systems are present, and also severe historical earthquakes are documented (Hammerl, 2017; Stucchi et al., 2013). Therefore, we propose that the scenarios A and D are likely to have happened in these regions near Imst and Innsbruck with the calculated minimum magnitudes of M_w 5.8 and 6.0, respectively (Fig. 7). With increasing distance and magnitude, the resulting magnitude and source area from the grid-search analysis cannot be further evaluated and narrowed down due to missing data points, which is especially the case for scenario A (towards the south; Fig. 6b) and scenario D (towards east and south; Fig. 6e). Plausible source areas of scenarios B (~ 4.1 ka) and C (~ 6.5 ka) are located at the northern part of the Fernpass–Loisach region (see considerations in Sect. 4.2), which is characterized by slightly increased seismicity within the generally seismically less active Alpine front (Fig. 6a; Reiter et al., 2018). It is conceivable that enough deformation is transferred towards the north and localized at this inherent, large-scale fault structure to generate severe earthquakes. However, the lack of present-day seismicity in the northern study area (Reiter et al., 2018) complicates the assessment of other potential active fault zones in the Alpine foreland despite the presence of major Alpine thrusts successively approaching the surface.

The ShakeMaps of selected paleo-earthquake scenarios provide first-order information that severe earthquakes within the western Austrian Alps also strongly affect large areas in the northern Alpine foreland in southern Germany. Several perialpine lakes are located in southern Germany, which are not yet studied for their potential paleoseismic

records but could essentially help in identifying more earthquake scenarios with multi-lake impact and help in better constraining epicenter locations and magnitudes of the scenarios proposed herein. A previous study at Ammersee found no earthquake imprints for the last 5.7 kyr (Czymzik et al., 2013). This contradicts the results of the ShakeMaps of the paleo-earthquake scenarios (Fig. 7), where at least two events have exceeded SI VII at Ammersee, which is above the upper threshold value to record seismic shaking in comparable Swiss perialpine lakes (Monecke et al., 2004). Either the sediments of Ammersee have a different susceptibility to failure during seismic shaking, or event horizons of multiple mass wasting remained undiscovered due to the lack of reflection seismic data or inadequate core siting to capture earthquake-related turbidites.

The proposed source areas of the paleo-earthquake scenarios A, B, and C (see argumentation in Sect. 4.2) potentially indicate a spatio-temporal migration of paleo-earthquakes from NE to SW in the area of the Fernpass–Loisach fault system (Fig. 8). When assuming these events ruptured on this fault system, this could indicate a progressive failure along this major fault structure similar to what is observed in some transform plate boundary regions, e.g., the North Anatolian Fault (Stein et al., 1997). Such stress redistribution patterns are not limited to active tectonic regions with high deformation rates but are also documented for the Friuli 1976 earthquake sequence in the Alps (Slejko, 2018). Yet, the interpretation of a progressive failure at the Fernpass–Loisach fault system might be biased by the fact that we can only estimate source areas for paleo-earthquakes that are recorded in at least two lakes. This interpretation ignores at least four paleo-earthquakes recorded only in Piburgersee between the 6.5 and the 4.1 ka events. However, these events are likely produced by a different fault source than the Fernpass–Loisach fault system, considering the missing coeval earthquake evidence in Plansee.

5.4 Potential implications of the paleoseismic catalogue of the western Austrian Alps

The three presented paleoseismic archives are located at different positions within the Alpine orogeny in terms of current seismicity (Fig. 6a), which is also reflected in their earthquake recurrence rates and patterns. We interpret the relatively shorter recurrence rates within the more inneralpine records Piburgersee and Achensee to be related to enhanced tectonic loading around the Inn valley also in prehistoric times. Hence, longer recurrence rates in the more external Plansee potentially reflect a decreased stress transfer across the current-day enhanced seismicity zone in the south. Additionally, recurrence behavior of the inneralpine records is slightly more aperiodic than the more external Plansee. This could reflect different processes increasingly affecting and modulating seismicity with increasing topography and elevation in the area of the inneralpine records, i.e., glacial isostatic adjustment, topographic potential energy, or erosion (Mazzotti et al., 2020). Especially a change in lithospheric stress due to postglacial unloading and isostatic rebound has been previously discussed to increase seismicity within the western Alps during Late Glacial to Early Holocene times (Beck et al., 1996; Kremer et al., 2017; Strasser et al., 2013). Without being able to resolve the processes modulating seismicity, increased seismicity related to postglacial unloading could potentially be indicated by the increased event frequency (822 years recurrence rate) between 12 and 16 ka at Plansee.

In comparison to the overall aperiodic recurrence patterns of other lacustrine paleoseismic records within the Alps (lakes Cadagno, Ledro, Bohinj, Savine, Lucerne, and Annecy compiled by Moernaut, 2020), the paleoseismic records of Tyrol are slightly more periodic, but with longer recurrence rates, except Lake Lucerne (recurrence interval = 2034 years, burstiness = -0.09), which is comparable to Plansee. The slightly more periodic recurrence behavior in the Tyrolean records could be partly artificial as records with low event numbers tend to underestimate the burstiness and thus tend towards a more periodic recurrence behavior (Kempf and Moernaut, 2021; Williams et al., 2019). However, the more regular earthquake recurrence pattern in Tyrol could indicate active deformation localization within one or only a few fault sources, whereas deformation in the other Alpine paleoseismic records is distributed over a complex system of interacting fault sources, which is more typical for intraplate tectonic settings (Liu et al., 2011). In Tyrol, the ca. 20 km broad and 100 km long zone of currently enhanced seismicity around the Inn valley is likely to mostly occur on a single active fault source or strongly interrelated fault sources linked in connection with activity at the sub-Tauern ramp (Ortner et al., 2006; Reiter et al., 2018). Additionally, constant tectonic loading of these faults is caused by ongoing 1–2 mm yr^{-1} northward pushing of the Adriatic microplate (Métois et al., 2015) located directly south of the study area.

The paleoseismic catalogue also provides insights into the spatio-temporal patterns of strong earthquake occurrence from the two inneralpine records Achensee and Piburgersee (Fig. 5a). A high event frequency (590-year recurrence rate) occurred at ~ 12 to ~ 8 ka at Achensee, during which only one event is documented at Piburgersee. In contrast, the period of ~ 7 to ~ 3 ka is characterized by a high event frequency (540 years recurrence rate) at Piburgersee and only two events in Achensee. Since then, three events are recorded in Achensee but none in Piburgersee. This observation potentially indicates a spatial shift in paleoseismicity from east to west to east in postglacial times. Strikingly, the proposed periods of enhanced seismicity at Achensee and Piburgersee both end with an outstanding severe earthquake, as documented by the size and number of their sedimentary imprints (Fig. 5a). Whether such a particularly severe earthquake significantly altered the local stress field by releasing a significant portion of energy accumulated by tectonic loading in

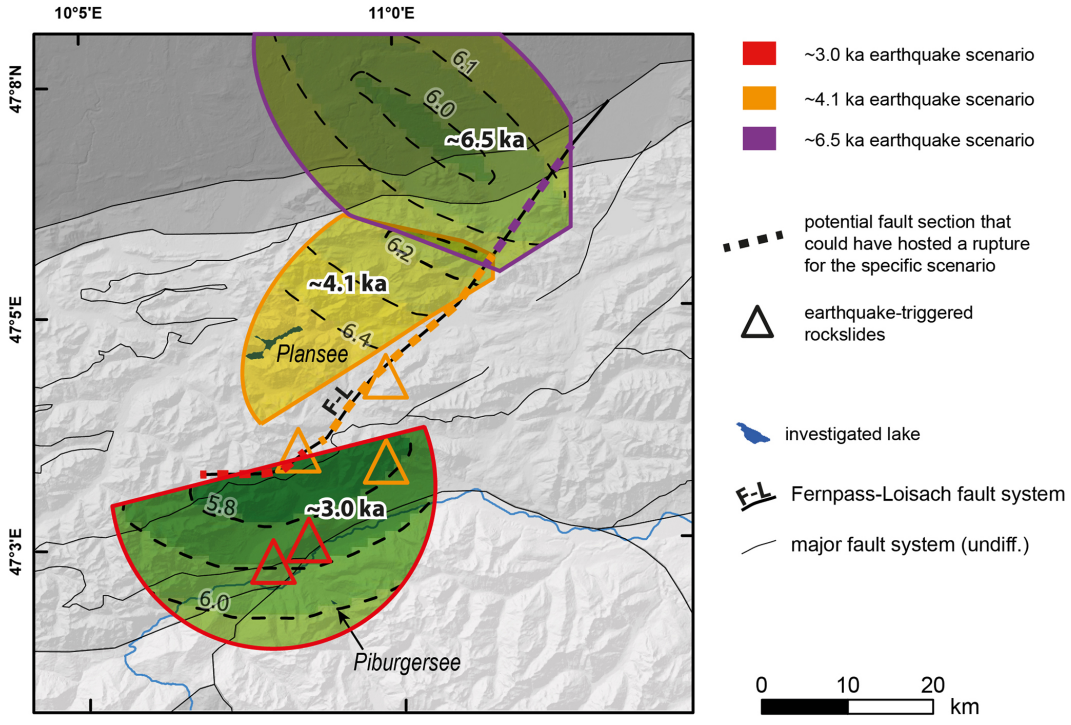

Figure 8. Potential NE–SW migration of severe earthquakes between ~ 6.5 and ~ 3.0 ka (paleo-earthquake scenarios A, B, and C) might indicate a progressive failure of the Fernpass–Loisach Fault. Solutions for the source area and minimum magnitude are derived from the inverse application of an IPE using the lacustrine paleoseismic evidence in a grid-search analysis (see Sect. 5.2 and Fig. 6).

the respective area or whether this observation is just coincidence cannot be resolved by the available number of paleoseismic archives.

A maximum credible earthquake magnitude of M_w 6 (+0.5 if a strike slip mechanism is involved) was previously assessed based on macroseismic data in this region (Lenhardt et al., 2007). The paleo-earthquake scenarios presented herein provide data-based observational evidence that an earthquake with a maximum credible magnitude, e.g., the M_w 6.0–6.3 at ~ 8.3 ka at Achensee, happened several times in the study area during the past 16 kyr. In particular, this has implications for the seismic demand in the building code of critical infrastructure such as dam structures, which are constructed based on the assessed maximum credible earthquake (Zenz and Obernhuber, 2002). In contrast, these findings do not have implications for the seismic design of general buildings and infrastructure (ÖNORM B 1998-1, 2011) as the recurrence interval of all three records combined (~ 630 years) is larger than the recurrence interval (475 years or 10 % probability of exceedance within 50 years) considered therein. However, it is left to future earthquake hazard assessments and policy makers to find adequate strategies to implement such low-frequency–high-impact scenarios, evaluate available mitigation and response strategies in the case of such a cross-border event, and prepare society also in intraplate tectonic regions for a possible worst-case scenario.

6 Conclusions

The first lacustrine paleoseismic archives of the western Austrian Alps revealed in total 25 earthquakes expressed as multiple coeval MTDs, SSDSs, or subaqueous surface ruptures. At the individual studied lake sites, seismic shaking with SI > VI 1/4 occurs every 1000–2000 years in a weakly periodic to aperiodic recurrence behavior. Severe paleo-earthquakes with minimum magnitudes of M_w 5.8–6.1 have occurred in the present-day zone of enhanced seismicity around the Inn valley, Brenner region, and Fernpass region, but also in the present-day low-seismicity zone of the upper Loisach region. A surface-rupturing earthquake at Achensee is constrained to M_w 6.0–6.3. NE–SW migration of paleo-earthquakes between ca. 6.5 and 3.0 ka might hint at a progressive failure along the Fernpass–Loisach Fault. Moreover, a shift in paleoseismicity from east to west to east in the area of the Inn valley during postglacial times might be indicated by the lacustrine paleoseismic archives. The ShakeMaps of paleo-earthquake scenarios highlight that severe earthquakes in the study area could strongly affect the northern foreland regions. Complementary paleoseismic investigations especially north and east of the study area are required to evaluate and further improve these initial results.

Code and data availability. Data and codes are available from the authors upon request.

Supplement. The supplement related to this article is available online at: https://doi.org/10.5194/nhess-22-2057-2022-supplement.

Author contributions. JM, MS, and PO designed the study. PO, JM, and MS acquired reflection seismic and core data, calculated earthquake recurrence statistics, generated the paleo-earthquake scenarios, and interpreted the results. JS wrote the code of the ShakeMaps. PO wrote the manuscript and produced the figures with input from all co-authors.

Competing interests. The contact author has declared that neither they nor their co-authors have any competing interests.

Disclaimer. Publisher's note: Copernicus Publications remains neutral with regard to jurisdictional claims in published maps and institutional affiliations.

Acknowledgements. We thank Markus Erhardt, Gerald Degenhart, and Wolfgang Recheis for the medical CT measurements at the Medical University of Innsbruck and Irka Hajdas for radiocarbon measurements. IHS Markit is acknowledged for their educational grant program providing the Kingdom seismic interpretation software. We thank the anonymous reviewer, Christian Beck, Lonnie Leithold, and Klaus Reicherter for their critical reviews on an earlier version of this paper.

Financial support. This research has been supported by the Tiroler Wissenschaftsförderung (TWF; grant no. UNI-16588/5-2019), the Austrian Science Fund (FWF; grant no. P30285-N34), and the Interreg (grant no. ITAT-3016).

Review statement. This paper was edited by Filippos Vallianatos and reviewed by Christian Beck and one anonymous referee.

References

Alsop, G. I. and Marco, S.: Soft-sediment deformation within seismogenic slumps of the Dead Sea Basin, J. Struct. Geol., 33, 433–457, https://doi.org/10.1016/j.jsg.2011.02.003, 2011.

Avşar, U., Jónsson, S., Avşar, Ö., and Schmidt, S.: Earthquake-induced soft-sediment deformations and seismically amplified erosion rates recorded in varved sediments of Köyceğiz Lake (SW Turkey), J. Geophys. Res.-Sol. Ea., 121, 4767–4779, https://doi.org/10.1002/2016JB012820, 2016.

Bakun, W. H. and Wentworth, C. M.: Estimating earthquake location and magnitude from seismic intensity data, B. Seismol. Soc. Am., 87, 1502–1521, 1997.

Beck, C.: Late Quaternary lacustrine paleo-seismic archives in north-western Alps: Examples of earthquake-origin assessment of sedimentary disturbances, Earth-Sci. Rev., 96, 327–344, https://doi.org/10.1016/j.earscirev.2009.07.005, 2009.

Beck, C., Manalt, F., Chapron, E., Van Rensbergen, P., and De Batist, M.: Enhanced seismicity in the early post-glacial period: Evidence from the post-würm sediments of lake annecy, northwestern Alps, J. Geodyn., 22, 155–171, https://doi.org/10.1016/0264-3707(96)00001-4, 1996.

Bellwald, B.: Paleoseismologic Implication Sof the Sediment Stratigraphy in Lake Silvaplana (Engadine, Eastern Switzerland), Master thesis, ETH Zürich, Zürich, 2012.

Bellwald, B., Hjelstuen, B. O., Sejrup, H. P., Stokowy, T., and Kuvås, J.: Holocene mass movements in west and mid-Norwegian fjords and lakes, Mar. Geol., 407, 192–212, https://doi.org/10.1016/j.margeo.2018.11.007, 2019.

Blaauw, M. and Christen, J. A.: Flexible paleoclimate age-depth models using an autoregressive gamma process, Bayesian Anal., 6, 457–474, https://doi.org/10.1214/11-BA618, 2011.

Brooks, G. R.: Deglacial record of palaeoearthquakes interpreted from mass transport deposits at three lakes near Rouyn-Noranda, north-western Quebec, Canada, Sedimentology, 65, 2439–2467, https://doi.org/10.1111/sed.12473, 2018.

Brooks, G. R. and Adams, J.: A review of evidence of glacially-induced faulting and seismic shaking in eastern Canada, Quaternary Sci. Rev., 228, 106070, https://doi.org/10.1016/j.quascirev.2019.106070, 2020.

Carulli, G. B. and Slejko, D.: The 1976 Friuli, Italy, Earthquake, G. di Geol. Appl., 1, 147–156, https://www.aigaa.org/public/GGA.2005-01.0-15.0015.pdf (last access: 15 June 2022), 2005.

Chassiot, L., Chapron, E., Di Giovanni, C., Albéric, P., Lajeunesse, P., Lehours, A.-C., and Meybeck, M.: Extreme events in the sedimentary record of maar Lake Pavin: Implications for natural hazards assessment in the French Massif Central, Quaternary Sci. Rev., 141, 9–25, https://doi.org/10.1016/j.quascirev.2016.03.020, 2016.

Czymzik, M., Brauer, A., Dulski, P., Plessen, B., Naumann, R., von Grafenstein, U., and Scheffler, R.: Orbital and solar forcing of shifts in Mid- to Late Holocene flood intensity from varved sediments of pre-alpine Lake Ammersee (southern Germany), Quaternary Sci. Rev., 61, 96–110, https://doi.org/10.1016/j.quascirev.2012.11.010, 2013.

Daut, G.: Subaquatische Massenbewegungen im Starnberger See und im Tegernsee, Münchner Geol. Hefte R. B Angew. Geol., B5, 121 pp., 1998.

de La Taille, C., Jouanne, F., Crouzet, C., Beck, C., Jomard, H., de Rycker, K., and van Daele, M.: Impact of active faulting on the post LGM infill of Le Bourget Lake (western Alps, France), Tectonophysics, 664, 31–49, https://doi.org/10.1016/j.tecto.2015.08.024, 2015.

Doughty, M., Eyles, N., Eyles, C. H., Wallace, K., and Boyce, J. I.: Lake sediments as natural seismographs: Earthquake-related deformations (seismites) in central Canadian lakes, Sediment. Geol., 313, 45–67, https://doi.org/10.1016/j.sedgeo.2014.09.001, 2014.

Eisbacher, G. H. and Brandner, R.: Superposed fold-thrust structures and high-angle faults, Northwestern Calcareous Alps, Austria, Eclogae Geol. Helv., 89, 553–571, 1996.

Fabbri, S. C., Herwegh, M., Horstmeyer, H., Hilbe, M., Hübscher, C., Merz, K., Schlunegger, F., Schmelzbach, C., Weiss, B., and Anselmetti, F. S.: Combining amphibious geomorphology with subsurface geophysical and geological data: A neotectonic study at the front of the Alps (Bernese Alps, Switzerland), Quatern. Int., 451, 101–113, https://doi.org/10.1016/j.quaint.2017.01.033, 2017.

Fabbri, S. C., Affentranger, C., Krastel, S., Lindhorst, K., Wessels, M., Madritsch, H., Allenbach, R., Herwegh, M., Heuberger, S., Wielandt-Schuster, U., Pomella, H., Schwestermann, T., and Anselmetti, F. S.: Active Faulting in Lake Constance (Austria, Germany, Switzerland) Unraveled by Multi-Vintage Reflection Seismic Data, Front. Earth Sci., 9, 1–26, https://doi.org/10.3389/feart.2021.670532, 2021.

Fäh, D., Giardini, D., Kästli, P., Deichmann, N., Gisler, M., Schwarz-Zanetti, G., Alvarez-Rubio, S., Sellami, S., Edwards, B., Allmann, B., Bethmann, F., Wössner, J., Gassner-Stamm, G., Fritsche, S., and Eberhard, D.: ECOS-09 Earthquake Catalogue of Switzerland Release 2011, Report and Database, Public catalogue, Swiss Seismological Service ETH Zürich, Report SED/RISK/R/001/20110417, http://www.seismo.ethz.ch/static/ecos-09/ECOS-2009_Report_final_WEB.pdf (last access: 28 August 2021), 2011.

Galadini, F. and Galli, P.: Palaeoseismology related to the displaced Roman archaeological remains at Egna (Adige Valley, northern Italy), Tectonophysics, 308, 171–191, https://doi.org/10.1016/S0040-1951(99)00080-3, 1999.

Gasperini, L., Marzocchi, A., Mazza, S., Miele, R., Meli, M., Najjar, H., Michetti, A. M., and Polonia, A.: Morphotectonics and late Quaternary seismic stratigraphy of Lake Garda (Northern Italy), Geomorphology, 371, 107427, https://doi.org/10.1016/j.geomorph.2020.107427, 2020.

Goh, K.-I. and Barabási, A.-L.: Burstiness and memory in complex systems, Europhys. Lett., 81, 48002, https://doi.org/10.1209/0295-5075/81/48002, 2008.

Griffin, J. D., Stirling, M. W., and Wang, T.: Periodicity and Clustering in the Long-Term Earthquake Record, Geophys. Res. Lett., 47, e2020GL089272, https://doi.org/10.1029/2020GL089272, 2020.

Grünthal, G.: European Macroseismic Scale 1998 EMS-98, Eur. Seismol. Comm. Subcomm. Eng. Seismol., Working Group Macroseismic Scales, Cons. l'Europe, Cah. du Cent. Eur. Géodynamique Séismologie, 99 pp., ISBN No2-87977-008-4, 1998.

Hammerl, C.: Historical earthquake research in Austria, Geosci. Lett., 4, 99, https://doi.org/10.1186/s40562-017-0073-8, 2017.

Hammerl, C., Lenhardt, W. A., and Innerkofler, M.: Forschungen zu den stärksten historischen Erdbeben im mittleren Inntal im Rahmen des INTERREG IV-Projekts HAREIA (Historical And Recent Earthquakes in Italy and Austria), Forum Hall Tirol. Neues zur Geschichte der Stadt, 3, 110–140, 2012.

Howarth, J. D., Fitzsimons, S. J., Norris, R. J., and Jacobsen, G. E.: Lake sediments record high intensity shaking that provides insight into the location and rupture length of large earthquakes on the Alpine Fault, New Zealand, Earth Planet. Sc. Lett., 403, 340–351, https://doi.org/10.1016/j.epsl.2014.07.008, 2014.

Howarth, J. D., Fitzsimons, S. J., Norris, R. J., Langridge, R., and Vandergoes, M. J.: A 2000 yr rupture history for the Alpine fault derived from Lake Ellery, South Island, New Zealand, Bull. Geol. Soc. Am., 128, 627–643, https://doi.org/10.1130/B31300.1, 2016.

Ivy-Ochs, S., Kerschner, H., Reuther, A., Preusser, F., Heine, K., Maisch, M., Kubik, P. W., and Schlüchter, C.: Chronology of the last glacial cycle in the European Alps, J. Quaternary Sci., 23, 559–573, 2008.

Kempf, P. and Moernaut, J.: Age uncertainty in recurrence analysis of paleoseismic records, J. Geophys. Res.-Sol. Ea., 126, e2021JB021996, https://doi.org/10.1029/2021JB021996, 2021.

Kiefer, C., Oswald, P., Moernaut, J., Fabbri, S. C., Mayr, C., Strasser, M., and Krautblatter, M.: A 4000-year debris flow record based on amphibious investigations of fan delta activity in Plansee (Austria, Eastern Alps), Earth Surf. Dynam., 9, 1481–1503, https://doi.org/10.5194/esurf-9-1481-2021, 2021.

Kremer, K., Wirth, S. B., Reusch, A., Fäh, D., Bellwald, B., Anselmetti, F. S., Girardclos, S., and Strasser, M.: Lake-sediment based paleoseismology: Limitations and perspectives from the Swiss Alps, Quaternary Sci. Rev., 168, 1–18, https://doi.org/10.1016/j.quascirev.2017.04.026, 2017.

Lauterbach, S., Chapron, E., Brauer, A., Hüls, M., Gilli, A., Arnaud, F., Piccin, A., Nomade, J., Desmet, M., von Grafenstein, U., and DecLakes Participants: A sedimentary record of Holocene surface runoff events and earthquake activity from Lake Iseo (Southern Alps, Italy), The Holocene, 22, 749–760, https://doi.org/10.1177/0959683611430340, 2012.

Lemaire, E., Mreyen, A.-S., Dufresne, A., and Havenith, H.-B.: Analysis of the Influence of Structural Geology on the Massive Seismic Slope Failure Potential Supported by Numerical Modelling, Geosciences, 10, 323, https://doi.org/10.3390/geosciences10080323, 2020.

Lenhardt, W. A., Freudenthaler, C., Lippitsch, R., and Fiegweil, E.: Focal-depth distributions in the Austrian Eastern Alps based on macroseismic data, Austrian J. Earth Sc., 100, 66–79, 2007.

Liu, M., Stein, S., and Wang, H.: 2000 years of migrating earthquakes in North China: How earthquakes in midcontinents differ from those at plate boundaries, Lithosphere, 3, 128–132, https://doi.org/10.1130/L129.1, 2011.

Mancktelow, N., Zwingmann, H., Campani, M., Fügenschuh, B., and Mulch, A.: Timing and conditions of brittle faulting on the Silltal-Brenner Fault Zone, Eastern Alps (Austria), Swiss J. Geosci., 108, 305–326, https://doi.org/10.1007/s00015-015-0179-y, 2015.

Mazzotti, S., Jomard, H., and Masson, F.: Processes and deformation rates generating seismicity in metropolitan France and conterminous Western Europe, BSGF – Earth Sci. Bull., 191, 19 pp., https://doi.org/10.1051/bsgf/2020019, 2020.

Métois, M., D'Agostino, N., Avallone, A., Chamot-Rooke, N., Rabaute, A., Duni, L., Kuka, N., Koci, R., and Georgiev, I.: Insights on continental collisional processes from GPS data: Dynamics of the peri-Adriatic belts, J. Geophys. Res.-Sol. Ea., 120, 8701–8719, https://doi.org/10.1002/2015JB012023, 2015.

Moernaut, J.: Time-dependent recurrence of strong earthquake shaking near plate boundaries: A lake sediment perspective, Earth-Sci. Rev., 210, 103344, https://doi.org/10.1016/j.earscirev.2020.103344, 2020.

Moernaut, J., van Daele, M., Heirman, K., Fontijn, K., Strasser, M., Pino, M., Urrutia, R., and de Batist, M.: Lacustrine turbidites as a tool for quantitative earthquake reconstruction: New evidence for a variable rupture mode in south

central Chile, J. Geophys. Res.-Sol. Ea., 119, 1607–1633, https://doi.org/10.1002/2013JB010738, 2014.

Molenaar, A., Van Daele, M., Vandorpe, T., Degenhart, G., De Batist, M., Urrutia, R., Pino, M., Strasser, M., and Moernaut, J.: What controls the remobilization and deformation of surficial sediment by seismic shaking? Linking lacustrine slope stratigraphy to great earthquakes in South–Central Chile, Sedimentology, 68, 2365–2396, https://doi.org/10.1111/sed.12856, 2021.

Monecke, K., Anselmetti, F. S., Becker, A., Sturm, M., and Giardini, D.: The record of historic earthquakes in lake sediments of Central Switzerland, Tectonophysics, 394, 21–40, https://doi.org/10.1016/j.tecto.2004.07.053, 2004.

ÖNORM B 1998-1: Eurocode 8: Auslegung von Bauwerken gegen Erdbeben. Teil 1: Grundlagen, Erdbebeneinwirkungen und Regeln für Hochbauten. Ausgabe 201106-15. Ersatz für ÖNORM EN 1998-1:2005-06, Austrian Standards Institute (ON), 2011.

Ortner, H., Reiter, F., and Brandner, R.: Kinematics of the Inntal shear zone-sub-Tauern ramp fault system and the interpretation of the TRANSALP seismic section, Eastern Alps, Austria, Tectonophysics, 414, 241–258, https://doi.org/10.1016/j.tecto.2005.10.017, 2006.

Oswald, P., Moernaut, J., Fabbri, S. C., De Batist, M., Hajdas, I., Ortner, H., Titzler, S., and Strasser, M.: Combined On-Fault and Off-Fault Paleoseismic Evidence in the Postglacial Infill of the Inner-Alpine Lake Achensee (Austria, Eastern Alps), Front. Earth Sci., 9, 438, https://doi.org/10.3389/feart.2021.670952, 2021a.

Oswald, P., Strasser, M., Hammerl, C., and Moernaut, J.: Seismic control of large prehistoric rockslides in the Eastern Alps, Nat. Commun., 12, 1059, https://doi.org/10.1038/s41467-021-21327-9, 2021b.

Petersen, J., Wilhelm, B., Revel, M., Rolland, Y., Crouzet, C., Arnaud, F., Brisset, E., Chaumillon, E., and Magand, O.: Sediments of Lake Vens (SW European Alps, France) record large-magnitude earthquake events, J. Paleolimnol., 51, 343–355, https://doi.org/10.1007/s10933-013-9759-x, 2014.

Plan, L., Grasemann, B., Spötl, C., Decker, K., Boch, R., and Kramers, J.: Neotectonic extrusion of the Eastern Alps: Constraints from U/Th dating of tectonically damaged speleothems, Geology, 38, 483–486, 2010.

Praet, N., Moernaut, J., van Daele, M., Boes, E., Haeussler, P. J., Strupler, M., Schmidt, S., Loso, M. G., and de Batist, M.: Paleoseismic potential of sublacustrine landslide records in a high-seismicity setting (south-central Alaska), Mar. Geol., 384, 103–119, https://doi.org/10.1016/j.margeo.2016.05.004, 2017.

Praet, N., Van Daele, M., Collart, T., Moernaut, J., Vandekerkhove, E., Kempf, P., Haeussler, P. J., and De Batist, M.: Turbidite stratigraphy in proglacial lakes: Deciphering trigger mechanisms using a statistical approach, Sedimentology, 67, 2332–2359, https://doi.org/10.1111/sed.12703, 2020.

Prager, C., Zangerl, C., Patzelt, G., and Brandner, R.: Age distribution of fossil landslides in the Tyrol (Austria) and its surrounding areas, Nat. Hazards Earth Syst. Sci., 8, 377–407, https://doi.org/10.5194/nhess-8-377-2008, 2008.

Ratschbacher, L., Merle, O., Davy, P., and Cobbold, P.: Lateral extrusion in the eastern Alps, Part 1: Boundary conditions and experiments scaled for gravity, Tectonics, 10, 245–256, https://doi.org/10.1029/90TC02622, 1991.

Reiter, F., Freudenthaler, C., Hausmann, H., Ortner, H., Lenhardt, W., and Brandner, R.: Active Seismotectonic Deformation in Front of the Dolomites Indenter, Eastern Alps, Tectonics, 37, 4625–4654, https://doi.org/10.1029/2017TC004867, 2018.

Rosenberg, C. L., Brun, J. P., and Gapais, D.: Indentation model of the Eastern Alps and the origin of the Tauern Window, Geology, 32, 997–1000, https://doi.org/10.1130/G20793.1, 2004.

Rudloff, A. and Leydecker, G.: Ableitung von empirischen Beziehungen zwischen der Lokalbebenmagnitude und makroseismischen Parametern-Ergebnisbericht, BGR, Hannover, https://scholar.google.at/scholar?hl=en&as_sdt=0%2C5&q=Rudloff+and+Leydecker+%282002%29+&btnG= (last access: 4 August 2021), 2002.

Schnellmann, M., Anselmetti, F. S., Giardini, D., Mckenzie, J. A., and Ward, S. N.: Prehistoric earthquake history revealed by lacustrine slump deposits, Geology, 30, 1131–1134, https://doi.org/10.1130/0091-7613(2002)030<1131:PEHRBL>2.0.CO;2, 2002.

Schwestermann, T.: Mass-movement event stratigraphy in lake constance, Master thesis, ETH Zürich, Zürich, 2016.

Serva, L., Vittori, E., Comerci, V., Esposito, E., Guerrieri, L., Michetti, A. M., Mohammadioun, B., Mohammadioun, G. C., Porfido, S., and Tatevossian, R. E.: Earthquake Hazard and the Environmental Seismic Intensity (ESI) Scale, Pure Appl. Geophys., 173, 1479–1515, https://doi.org/10.1007/s00024-015-1177-8, 2016.

Simonneau, A., Chapron, E., Vannière, B., Wirth, S. B., Gilli, A., Di Giovanni, C., Anselmetti, F. S., Desmet, M., and Magny, M.: Mass-movement and flood-induced deposits in Lake Ledro, southern Alps, Italy: implications for Holocene palaeohydrology and natural hazards, Clim. Past, 9, 825–840, https://doi.org/10.5194/cp-9-825-2013, 2013.

Slejko, D.: What science remains of the 1976 Friuli earthquake?, B. Geofis. Teor. Appl., 59, 327–350, https://doi.org/10.4430/bgta0224, 2018.

Sponheuer, W.: Methoden zur Herdtiefenbestimmung in der Makroseismik, Akademie-Verlag, Berlin, https://scholar.google.at/scholar?hl=en&as_sdt=0%2C5&q=Sponheuer%2C+W.+%281960%29+Methoden+zur+Herdtiefenbestimmung+in+der+Makroseismik.+Freiberger+Forschungs-Hefte%2C+C88%2C+120+S.&btnG= (last access: 4 August 2021), 1960.

Stein, R. S., Barka, A. A., and Dieterich, J. H.: Progressive failure on the North Anatolian fault since 1939 by earthquake stress triggering, Geophys. J. Int., 128, 594–604, 1997.

Stirling, M., Rhoades, D., and Berryman, K.: Comparison of Earthquake Scaling Relations Derived from Data of the Instrumental and Preinstrumental Era, B. Seismol. Soc. Am., 92, 812–830, https://doi.org/10.1785/0120000221, 2002.

Strasser, M. and Anselmetti, F.: Mass-movement event stratigraphy in Lake Zurich; a record of varying seismic and environmental impacts, Beiträge zur Geol. Schw., Geotechn. Ser, 95, 23–41, http://scholar.google.com/scholar?hl=en&btnG=Search&q=intitle:MASS-MOVEMENT+EVENT+STRATIGRAPHY+IN+LAKE+ZURICH:+A+RECORD+OF+VARYING+SEISMIC+AND+ENVIRONMENTAL+IMPACTS#0 (last access: 25 September 2021), 2008.

Strasser, M., Anselmetti, F. S., Fäh, D., Giardini, D., and Schnellmann, M.: Magnitudes and source areas of large prehistoric

northern Alpine earthquakes revealed by slope failures in lakes, Geology, 34, 1005, https://doi.org/10.1130/G22784A.1, 2006.

Strasser, M., Monecke, K., Schnellmann, M., and Anselmetti, F. S.: Lake sediments as natural seismographs: A compiled record of Late Quaternary earthquakes in Central Switzerland and its implication for Alpine deformation, Sedimentology, 60, 319–341, https://doi.org/10.1111/sed.12003, 2013.

Stucchi, M., Rovida, A., Gomez Capera, A. A., Alexandre, P., Camelbeeck, T., Demircioglu, M. B., Gasperini, P., Kouskouna, V., Musson, R. M. W., Radulian, M., Sesetyan, K., Vilanova, S., Baumont, D., Bungum, H., Fäh, D., Lenhardt, W., Makropoulos, K., Martinez Solares, J. M., Scotti, O., Živčić, M., Albini, P., Batllo, J., Papaioannou, C., Tatevossian, R., Locati, M., Meletti, C., Viganò, D., and Giardini, D.: The SHARE European Earthquake Catalogue (SHEEC) 1000–1899, J. Seismol., 17, 523–544, https://doi.org/10.1007/s10950-012-9335-2, 2013.

Ustaszewski, M. and Pfiffner, O. A.: Neotectonic faulting, uplift and seismicity in the central and western Swiss Alps, Geol. Soc. Spec. Publ., 298, 231–249, https://doi.org/10.1144/SP298.12, 2008.

Van Daele, M., Moernaut, J., Doom, L., Boes, E., Fontijn, K., Heirman, K., Vandoorne, W., Hebbeln, D., Pino, M., Urrutia, R., Brümmer, R., and De Batist, M.: A comparison of the sedimentary records of the 1960 and 2010 great Chilean earthquakes in 17 lakes: Implications for quantitative lacustrine palaeoseismology, Sedimentology, 62, 1466–1496, https://doi.org/10.1111/sed.12193, 2015.

Van Daele, M., Haeussler, P. J., Witter, R. C., Praet, N., and De Batist, M.: The sedimentary record of the 2018 Anchorage earthquake in Eklutna Lake, Alaska: Calibrating the lacustrine seismograph, Seismol. Res. Lett., 91, 126–141, https://doi.org/10.1785/0220190204, 2019.

Vanneste, K., Wils, K., and Van Daele, M.: Probabilistic Evaluation of Fault Sources Based on Paleoseismic Evidence From Mass-Transport Deposits: The Example of Aysén Fjord, Chile, J. Geophys. Res.-Sol. Ea., 123, 9842–9865, https://doi.org/10.1029/2018JB016289, 2018.

Vasskog, K., Nesje, A., Støren, E. N., Waldmann, N., Chapron, E., and Ariztegui, D.: A Holocene record of snow-avalanche and flood activity reconstructed from a lacustrine sedimentary sequence in Oldevatnet, western Norway, The Holocene, 21, 597–614, https://doi.org/10.1177/0959683610391316, 2011.

Wetzler, N., Marco, S., and Heifetz, E.: Quantitative analysis of seismogenic shear-induced turbulence in lake sediments, Geology, 38, 303–306, https://doi.org/10.1130/G30685.1, 2010.

Wilhelm, B., Nomade, J., Crouzet, C., Litty, C., Sabatier, P., Belle, S., Rolland, Y., Revel, M., Courboulex, F., Arnaud, F., and Anselmetti, F. S.: Quantified sensitivity of small lake sediments to record historic earthquakes: Implications for paleoseismology, J. Geophys. Res.-Earth, 121, 2–16, https://doi.org/10.1002/2015JF003644, 2016.

Williams, R. T., Davis, J. R., and Goodwin, L. B.: Do Large Earthquakes Occur at Regular Intervals Through Time? A Perspective From the Geologic Record, Geophys. Res. Lett., 46, 8074–8081, https://doi.org/10.1029/2019GL083291, 2019.

Wils, K., Deprez, M., Kissel, C., Vervoort, M., Van Daele, M., Daryono, M. R., Cnudde, V., Natawidjaja, D. H., and De Batist, M.: Earthquake doublet revealed by multiple pulses in lacustrine seismo-turbidites, Geology, 49, 1301–1306, https://doi.org/10.1130/G48940.1, 2021.

Zenz, G. and Obernhuber, P.: Erdbebenberechnung von Talsperren in Österreich, Wasserwirtschaft, 92, 2–8, 2002.

Zimmermann, J.: Der Walensee – eine sedimentologische Rekonstruktion seiner holozäanen Ereignisgeschichte, Master thesis, EAWAG, Zürich, 2008.